



HAL
open science

The response of a 2D droplet on a wall executing small sinusoidal vibrations

Julian F. Scott, Zlatko Solomenko, Peter D.M. Spelt

► **To cite this version:**

Julian F. Scott, Zlatko Solomenko, Peter D.M. Spelt. The response of a 2D droplet on a wall executing small sinusoidal vibrations. *International Journal of Multiphase Flow*, 2021, 142, pp.103732. 10.1016/j.ijmultiphaseflow.2021.103732 . hal-03573257

HAL Id: hal-03573257

<https://hal.science/hal-03573257>

Submitted on 7 Apr 2022

HAL is a multi-disciplinary open access archive for the deposit and dissemination of scientific research documents, whether they are published or not. The documents may come from teaching and research institutions in France or abroad, or from public or private research centers.

L'archive ouverte pluridisciplinaire **HAL**, est destinée au dépôt et à la diffusion de documents scientifiques de niveau recherche, publiés ou non, émanant des établissements d'enseignement et de recherche français ou étrangers, des laboratoires publics ou privés.

The response of a 2D droplet on a wall executing small sinusoidal vibrations

Abbreviated title: Droplet on a vibrating wall

Julian F. Scott, Zlatko Solomenko, Peter D.M. Spelt¹

Laboratoire de Mécanique des Fluides et d'Acoustique (LMFA), Université de Lyon, France

Summary

This study concerns a two-dimensional liquid drop surrounded by gas and attached to a sinusoidally vibrating wall. Gravity is neglected and the moving contact lines are modelled using a Navier-type boundary condition at the wall and a prescribed contact angle, $\bar{\theta}$, which can take any value in the range $0 < \bar{\theta} < \pi$. The vibration amplitude, and hence the departure from equilibrium of the drop, is assumed sufficiently small that the problem can be linearized. Wall vibration can have components both normal and tangential to the wall. The solution of the linear problem can be expressed as the sum of two decoupled components corresponding to the response to purely normal and purely tangential vibration, which are respectively symmetric and antisymmetric with respect to reflection in the symmetry plane of the equilibrium drop. Asymptotic analysis of the drop oscillations for small Ohnesorge number, Oh , brings out two distinct damping mechanisms, both of which are accounted for. One, arising from viscous dissipation in the regions near the contact lines, is characterized by a parameter β . The other comes from the boundary layer at the wall and is of order $Oh^{1/2}$. The small- Oh problem has been implemented numerically. As expected, lightly damped normal modes are found to have resonant response close to their inviscid oscillation frequencies. Damping coefficients for each of the two damping mechanisms and lightly damped modes are determined as a function of contact angle. The relative importance of boundary-layer and contact-line damping is quantified and found to depend both on the contact angle and on $\beta/Oh^{1/2}$. Cases can be found in which the two damping mechanisms have comparable effects, as well as others for which one or other of the mechanisms is dominant. Comparison with DNS, which allows for nonlinear effects and has the same contact-line model, shows agreement for a particular case having small Oh and small wall displacement amplitude.

Keywords: Drop vibration, resonance, damping, moving contact lines, numerical simulation.

1. Introduction

Studies of the free oscillations of a spherical drop of liquid surrounded by a gas go back a long way (see Rayleigh (1879) for the inviscid case and Lamb (1932), section 355 for the damping due to small viscosity). Such drops have normal modes with certain natural frequencies and damping rates. If the damping is weak, when subjected to small sinusoidal forcing, they respond strongly at their natural frequencies, i.e. there is resonance.

¹ Peter passed away on June 28, 2020. He will be sadly missed.

Constraints on the drop, such as the plane wall to which the drop is attached in the present problem, which is the case we focus on here, modify both the modal frequencies and damping. If the Ohnesorge number, which measures the importance of viscosity in the bulk of the drop, is small, the change in frequencies is an essentially inviscid effect due to the imposed normal velocity at the wall. Damping is increased significantly by the wall and arises from two regions: a boundary layer at the wall and the neighbourhood of the contact line. Both mechanisms appear in Hocking's (1987) analysis of the somewhat different problem of the damping of capillary-gravity waves confined between solid walls. Note that Hocking assumed a static contact angle of $\pi/2$, an assumption which is not made here, allowing us to study the effects of varying the angle.

A number of articles have studied the response of drops attached to a wall and subject to harmonic forcing. For example, Noblin *et al.* (2004) and Vukasinovic *et al.* (2007) report results of experimental work on spherical drops forced by sinusoidal vibrations normal to the wall. The first of these papers focuses on the transition between a pinned and moving contact line which can occur as the wall amplitude and frequency are varied. The second identifies different regimes of drop response as the amplitude is increased. Moradi *et al.* (2019) numerically studied the ejection of a drop from a smooth, normally vibrating wall. They found that the wall vibration amplitude above which ejection occurs, divided by the drop size, depends mainly on the vibration frequency and contact angle, drop ejection being favoured by frequencies near resonance and higher contact angles. Given the small-amplitude assumption of the present work, only the simplest regime, for which the drop responds at the wall frequency and there is no drop ejection, is relevant here.

Oh *et al.* (2012) present a DNS study in which the drop is forced, not by wall vibration, but by imposing an oscillatory contact angle at the wall. They find that the flow consists of a component which oscillates with the forcing frequency and another which is steady. The latter is due to finite-amplitude effects and is not covered by the small-amplitude, linearized model developed here. Brunet and Costalonga (2020) experimentally study the case in which vibration has components both normal and tangential to the wall. They quantify the interesting result that the drop can have both oscillations and a net motion along the wall. The latter is, of course, a finite-amplitude effect, which the present model does not include. Finally, the theoretical work by Lyubimov *et al.* (2006), which is the closest to our own we have found, concerns a spherical drop on a plane wall with sinusoidal vibrations. The static contact angle was assumed to be $\pi/2$ and the vibrations normal to the wall, hence a symmetric response. Neither assumption is made here. Despite their focus on diverse physical aspects of drop response, all six papers cited in this and the previous paragraph (and others not referenced here) illustrate the importance of resonant behaviour as the frequency is varied. This paper aims to develop a predictive model of the drop response to small amplitude wall oscillations, with particular emphasis on resonance.

The oscillations of a drop attached to a wall generally involve moving contact lines. Such flows are problematic because the usual model of fluid motion, i.e. the Navier-Stokes equations with a no-slip condition at the wall, leads to an unacceptable singularity at the contact line (see e.g. Moffatt (1964), Huh and Scriven (1971)). Although there is no agreed

definitive model of this situation (Bonn *et al.* (2009)), a frequently used one allows slip at the wall via a Navier condition in which slip is proportional to the shear rate, the constant of proportionality being referred to as the slip length and denoted λ . In this model the angle (contact angle) at which the liquid/gas interface meets the wall has a prescribed value $0 < \bar{\theta} < \pi$, which is a constant for the homogeneous wall of this article. This is the model used here. It cannot, of course, describe the stick-slip behaviour of the contact line found by Noblin *et al.* (2004) and other studies for some wall surfaces in certain parameter regimes.

In such a model, the slip length is small, which leads to different matched asymptotic regions, the smallest of which being the slip region, for which the distance from the contact line is $O(\lambda)$. Outside this region, the usual no-slip condition applies. In addition to his notable later work on the lubrication approximation (see Hocking (1981)), an analysis of the slip region was given by Hocking (1977) (c.f. Scott (2020)), while Hocking and Rivers (1982) used matched asymptotic expansions to study the slow spreading of a liquid droplet on a plane wall. Although problems like the present one cannot be described as slow spreading, the idea of matching of an outer region, away from contact lines, to regions close to the contact lines to obtain boundary conditions for the outer problem has more general applicability (Cox (1986)).

The problem considered here is the response of a two-dimensional (i.e. cylindrical, rather than spherical) drop attached to a wall having small sinusoidal oscillations perpendicular to the drop axis. Although this two-dimensional problem is less realistic than the three-dimensional one of a spherical drop (whose theoretical formulation is discussed in appendix E (supplementary material)), it allows the construction of a numerically tractable model in the limit of small Ohnesorge number, the advantage of the model being the greatly reduced numerical costs compared with DNS. This allows treatment of many more different parameter sets in a reasonable time on a PC, compared to lengthy runs on a supercomputer using DNS.

In the model, gravity is neglected. Given the small vibration amplitude, the governing equations (Navier-Stokes) and boundary conditions of the perturbation to equilibrium are linearized. The part of the drop away from the contact lines is referred to as the outer region. Because λ is small, the no-slip condition applies at the wall in this region. Analysis of the flow near the contact lines and matching to the outer region yields boundary conditions for that region. Wall vibration can have components both normal and tangential to the wall and the contact angle can take any value in the range $0 < \bar{\theta} < \pi$. The solution of the problem can be expressed as the sum of two decoupled components corresponding to the response to purely normal and purely tangential vibration. The former is symmetric, whereas the latter is antisymmetric, with respect to reflection in the symmetry plane of the equilibrium drop. The antisymmetric problem can be rather different from the symmetric one. This is because, in the inviscid case, the drop has no means of sensing tangential wall motion. Thus, it remains in equilibrium, unaffected by vibration. Viscosity allows vibration to affect the drop. However, in the symmetric case, the vibrations are normal to the wall and the drop is affected, even in the absence of viscosity.

The case of small Ohnesorge number is the only one for which we have developed a numerical implementation. In that case, the flow is essentially inviscid over the bulk of the drop, with viscous effects concentrated in a wall boundary layer and near the contact lines. Asymptotic analysis of the boundary layer and matching to the inviscid region gives wall boundary conditions for the outer region. Conditions on the liquid/gas interface are also derived and turn out to be inviscid to the order $(\text{Oh}^{1/2})$ to which the analysis is carried out. Thus, viscosity enters into the small-Oh outer problem via the wall and contact-line boundary conditions.

The paper is organized as follows. Section 2 describes the overall mathematical model, section 3 derives the linearized equations for small perturbations to equilibrium and section 4 specializes to sinusoidal wall motion. Section 5 presents an analysis of the limit of small Oh, the detailed numerical implementation of which is described in the supplementary material, appendices C and D. Section 6 compares some results of the model with DNS, while section 7 gives an analysis of the resonant response of lightly damped modes. Finally, section 8 gives results of the model.

2. Problem formulation

A two-dimensional liquid drop, attached to a vibrating plane wall, is surrounded by gas which is supposed inviscid and of constant pressure, p_a . Gravity is neglected and the liquid/gas interfacial surface tension, σ , is assumed constant, as are the liquid density and dynamic viscosity, ρ and μ . We use the reference frame of the wall and nondimensionalize throughout using L , $(\rho L^3 / \sigma)^{1/2}$, $(\sigma / \rho L)^{1/2}$, σ / L as length, time, velocity and pressure scales, where L is the length scale which gives a nondimensional drop area equal to 1. The Navier-Stokes equations in the liquid are

$$\frac{\partial \mathbf{u}}{\partial t} + \mathbf{u} \cdot \nabla \mathbf{u} = -\nabla p + \text{Oh} \nabla^2 \mathbf{u} - \mathbf{a}(t), \quad (2.1)$$

$$\nabla \cdot \mathbf{u} = 0, \quad (2.2)$$

where $\text{Oh} = \mu / (\sigma \rho L)^{1/2}$ is an Ohnesorge number and $\mathbf{a}(t)$ is the nondimensional acceleration of the wall in the inertial frame of reference. Note that, in general, \mathbf{a} may have both normal and tangential components. The vibrational term in (2.1) can be absorbed into the pressure gradient by defining an effective pressure as $p_e = p + \mathbf{a} \cdot \mathbf{x}$, where $\mathbf{x} = (x, y)$ and the Cartesian coordinates, x and y , are such that the wall lies at $y = 0$ and the drop in $y > 0$. Thus,

$$\frac{\partial \mathbf{u}}{\partial t} + \mathbf{u} \cdot \nabla \mathbf{u} = -\nabla p_e + \text{Oh} \nabla^2 \mathbf{u}. \quad (2.3)$$

The wall condition is

$$\lambda \frac{\partial u_x}{\partial y} = u_x, \quad u_y = 0 \quad y = 0, \quad (2.4)$$

where λ is the slip length, while the angle at which the liquid/gas interface meets the wall has the prescribed value $0 < \bar{\theta} < \pi$. The boundary conditions

$$\frac{\partial F}{\partial t} + \mathbf{u} \cdot \nabla F = 0, \quad (2.5)$$

$$\text{Oh} \mathbf{n} \cdot (\nabla \mathbf{u} + (\nabla \mathbf{u})^T) = \mathbf{n} (p_e - p_a - \kappa - \mathbf{a} \cdot \mathbf{x}) \quad (2.6)$$

apply at the interface, which is described by $F(\mathbf{x}, t) = 0$. Here, κ is the interface curvature and \mathbf{n} a unit normal vector to the interface, which is directed from the liquid towards the gas. Note that we have in mind that λ in (2.4) is small and that significant slip only occurs in regions, of size $O(\lambda)$, near the contact lines.

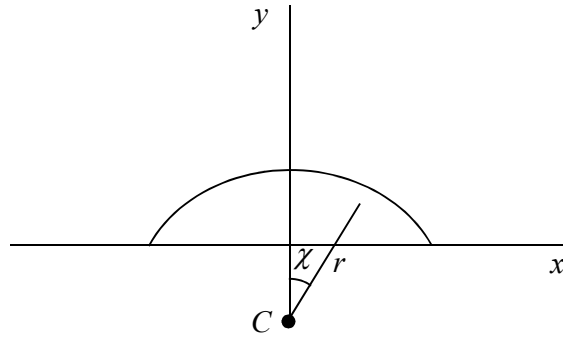


Figure 1: The equilibrium liquid/gas interface and associated polar coordinates. The interface is a circular arc of radius \bar{r} , centred at C .

When $\mathbf{a} = 0$, the drop has equilibria for which the contact-line positions, $x = \bar{x}_{\pm}$, are separated by

$$\bar{x}_+ - \bar{x}_- = \frac{2 \sin \bar{\theta}}{(\bar{\theta} - \sin \bar{\theta} \cos \bar{\theta})^{1/2}}. \quad (2.7)$$

The equilibrium interface is a circular arc, which intersects the wall with angle $\bar{\theta}$. For a given $\bar{\theta}$, there are infinitely many such equilibria, differing only by their displacement in x . In what follows, we choose the equilibrium which is symmetric about $x = 0$, i.e. $\bar{x}_- = -\bar{x}_+$. The resulting interface is shown in figure 1, as are associated polar coordinates, r, χ . The equilibrium interface is defined by $r = \bar{r}$ and $-\bar{\theta} \leq \chi \leq \bar{\theta}$, where $\bar{r} = (\bar{\theta} - \sin \bar{\theta} \cos \bar{\theta})^{-1/2}$ is

the equilibrium drop radius. The interface of the actual drop lies at $r = \bar{r} + \eta(\chi, t)$. Thus, η represents the perturbation of the interfacial location and we can choose $F(\mathbf{x}, t) = r - \bar{r} - \eta(\chi, t)$.

In the equilibrium state, $\kappa = \bar{r}^{-1}$ and $p_e = p_a + \bar{r}^{-1}$. Thus, (2.3) and (2.6) can be rewritten as

$$\frac{\partial \mathbf{u}}{\partial t} + \mathbf{u} \cdot \nabla \mathbf{u} = -\nabla p' + \text{Oh} \nabla^2 \mathbf{u}, \quad (2.8)$$

$$\text{Oh} \mathbf{n} \cdot \left(\nabla \mathbf{u} + (\nabla \mathbf{u})^T \right) = \mathbf{n} \cdot (p' - \kappa' - \mathbf{a} \cdot \mathbf{x}), \quad (2.9)$$

where $p' = p_e - p_a - \bar{r}^{-1}$, $\kappa' = \kappa - \bar{r}^{-1}$ are the difference between the actual values of p_e , κ and their values at equilibrium. The quantities \mathbf{u} , p' and η , which represent the perturbation to equilibrium, are governed by (2.2), (2.8), the boundary conditions, (2.4) at the wall, (2.5) and (2.9) at the interface, as well as the requirement that the interface meet the wall with angle $\bar{\theta}$. Note that wall vibration only appears via the term $\mathbf{a} \cdot \mathbf{x}$ in (2.9).

Before moving on, some remarks concerning the assumptions made in this paper are perhaps in order. Neglect of gravity requires a small Bond number, $\text{Bo} = \rho g L^2 / \sigma$, while, from section 5 onwards, we suppose small Oh. Small Bo and Oh respectively imply $L \ll (\sigma / \rho g)^{1/2}$ and $L \gg \mu^2 / \sigma \rho$, conditions which are only compatible if $\mu^2 (g / (\sigma^3 \rho))^{1/2} \ll 1$. For pure water at 20°C and $g = 9.81 \text{ms}^{-2}$, $\mu^2 (g / (\sigma^3 \rho))^{1/2} = 5 \times 10^{-6}$ and the applicability conditions are $L \ll 3 \times 10^{-3} \text{m}$ for neglect of gravity and $L \gg 1.4 \times 10^{-8} \text{m}$ for Oh $\ll 1$.

3. Small vibrations

From here on, we suppose \mathbf{a} , \mathbf{u} , p' and η small, thus linearizing the equations. (2.8) gives

$$\frac{\partial \mathbf{u}}{\partial t} = -\nabla p' + \text{Oh} \nabla^2 \mathbf{u}. \quad (3.1)$$

Using $F(\mathbf{x}, t) = r - \bar{r} - \eta(\chi, t)$, (2.5) implies

$$\frac{\partial \eta}{\partial t} + \frac{1}{\bar{r} + \eta} u_\chi \frac{\partial \eta}{\partial \chi} = u_r. \quad (3.2)$$

The term containing u_χ is second order in the perturbation and is therefore neglected. Furthermore, \mathbf{n} is in the r -direction for the unperturbed interface, thus, to first order,

$$\frac{\partial \eta}{\partial t} = \mathbf{u} \cdot \mathbf{n} \quad (3.3)$$

on the interface. κ' is expressed to first order in η in section A.1:

$$\kappa' = -\frac{1}{\bar{r}^2} \left(\frac{\partial^2 \eta}{\partial \chi^2} + \eta \right). \quad (3.4)$$

(3.4) is used in the normal component of (2.9) to obtain

$$\text{Oh } \mathbf{n} \cdot \left(\nabla \mathbf{u} + (\nabla \mathbf{u})^T \right) \cdot \mathbf{n} = p' + \frac{1}{\bar{r}^2} \left(\frac{\partial^2 \eta}{\partial \chi^2} + \eta \right) - \mathbf{a} \cdot \mathbf{x}, \quad (3.5)$$

while the tangential component of (2.9) gives

$$\mathbf{n} \cdot \left(\nabla \mathbf{u} + (\nabla \mathbf{u})^T \right) \cdot \mathbf{t} = 0, \quad (3.6)$$

where \mathbf{t} is a unit tangent vector of the interface. Note that, because the perturbation of the interface is small in the linearized problem, (3.3), (3.5) and (3.6) are applied on the equilibrium interface, $r = \bar{r}$, and \mathbf{n} and \mathbf{t} have their equilibrium values.

Turning attention to the flow near the contact lines, the requirement that the interface meet the wall with angle $\bar{\theta}$ can be expressed as $n_y = \cos \bar{\theta}$ or equivalently

$$n_r \cos \chi - n_\chi \sin \chi = \cos \bar{\theta} \quad (3.7)$$

at the contact lines. The contact line which lies at $\chi = \pm \bar{\theta}$ in the equilibrium state has the perturbed value $\chi = \pm \left(\bar{\theta} + \eta_\pm \bar{r}^{-1} \cot \bar{\theta} \right)$, correct to first order in the perturbation, where η_\pm is the contact-line value of η . Note that, here and henceforth, given a choice of signs, the upper one corresponds to the right-hand contact line, while the lower one corresponds to the left-hand contact line. Using this result and (A.3), (3.7) implies

$$\frac{\partial \eta}{\partial \chi} = \pm \eta_\pm \cot \bar{\theta} \quad (3.8)$$

at the contact lines. Appendix B gives an analysis of the flow close to a contact line, using (3.8) and leading to

$$\frac{1}{\bar{r}} \frac{\partial \eta}{\partial \chi} \sim \pm \left(\eta_\pm \frac{\cot \bar{\theta}}{\bar{r}} - \frac{d\eta_\pm}{dt} \frac{2 \text{Oh}}{\bar{\theta} - \sin \bar{\theta} \cos \bar{\theta}} \ln \left(\frac{R}{\tilde{\lambda}} \right) \right), \quad (3.9)$$

where $\lambda \ll R \ll 1$ is the distance from the contact line and $\tilde{\lambda}$ is an effective slip length, which is an $O(1)$ multiple of λ , the multiplying factor being a function of $\bar{\theta}$. Thus, $\tilde{\lambda}$ is constant for a given drop. (3.9) indicates a logarithmic dependency on R outside the slip

region and applies for small R , sufficiently small that the unsteady term in (3.1) can be neglected, but not so small as to be comparable with λ . The factor Oh in the logarithmic term expresses its viscous origin.

(3.9) corresponds to nondimensionalisation of equation (4.7) of Hocking and Rivers (1982). In particular, the logarithmic term agrees (to within a choice of signs which comes from relating $\bar{r}^{-1}\partial\eta/\partial\chi$ to the interface-slope angle, as does the remaining term on the right-hand side of (3.9)) with the second term on the right-hand side of their equation (the nondimensional contact-line advancement velocity being $\frac{1}{\sin\bar{\theta}}\frac{d\eta_{\pm}}{dt}$). $(\sin\bar{\theta})^{-1}d\eta_{\pm}/dt$ It should be noted that (4.7) of the above reference expresses matching of the intermediate and slip regions, i.e. it holds as the contact line is approached from $R \gg \lambda$. However, given the small perturbation to equilibrium in our problem, the slope angle is close to $\bar{\theta}$ for all $R \ll 1$. In consequence, the analysis in section 5 of the above reference, which takes into account variations of the slope angle near the contact line, is unnecessary and (4.7) of the above reference, or equivalently our equation (3.9), applies for all $\lambda \ll R \ll 1$.

Define the outer region as the interior of the equilibrium drop away from the contact lines, i.e. $R = O(1)$ for both lines. Because λ is small, slip is negligible in the outer region and the wall boundary condition is

$$\mathbf{u} = 0 \quad y = 0. \quad (3.10)$$

Matching to the region $\lambda \ll R \ll 1$, (3.9) applies as $R \rightarrow 0$ from the outer region. The outer-region problem consists of (2.2), (3.1) and the boundary conditions (3.3), (3.5) and (3.6) on $r = \bar{r}$, (3.9) as $R \rightarrow 0$ and (3.10) at the wall. Initial conditions, consisting of a specification of η and \mathbf{u} , are also needed to complete the problem. Because the nondimensionalisation is such that both the equilibrium and perturbed drops have the same area,

$$\int_{-\bar{\theta}}^{\bar{\theta}} \eta d\chi = 0. \quad (3.11)$$

(3.11) constrains the initial η . Integration of (2.2) over the drop and use of the divergence theorem, $u_y = 0$ at the wall and (3.3) on $r = \bar{r}$ shows that the left-hand side of (3.11) is independent of time, an expression of drop area conservation. Thus, because (3.11) is satisfied at the initial instant, it automatically holds at all subsequent times.

When $\mathbf{a} = 0$, the problem has complex solutions with exponential time dependence. Such solutions are often referred to as modes. Taking \mathbf{u} , p' and η as products of e^{st} and functions of \mathbf{x} leads to an eigenvalue problem with eigenvalue s . The general solution of the linearized problem consists of a sum over modes. One mode has $s = 0$, $\mathbf{u} = 0$, $p' = 0$ and

$$\eta = C \sin \chi, \quad (3.12)$$

where C is an arbitrary real constant. This solution corresponds to a slightly different equilibrium, obtained from the chosen one by a small displacement parallel to the wall. The general solution with $\mathbf{a} = 0$ consists of the sum of (3.12) and a combination of $s \neq 0$ modes. Viscous damping means that such modes are decaying; thus, if $\mathbf{a} = 0$, the end result as $t \rightarrow \infty$ is (3.12), as might be expected. Viscosity is always present in reality, but it can be artificially removed by setting $\text{Oh} = 0$. This has the effect of making the eigenvalues purely imaginary, thus the $s \neq 0$ inviscid modes oscillate sinusoidally without decay. Note that, with or without viscosity, the modes form complex conjugate pairs.

4. Sinusoidal vibration

Up to now the wall vibration has not been specified, whereas henceforth we consider sinusoidal vibration, $\mathbf{a}(t) = \Re(\tilde{\mathbf{a}}e^{i\varpi t})$, where $\tilde{\mathbf{a}}$ is complex and $\varpi \neq 0$ is real. The outer problem has a particular solution of the form

$$\mathbf{u} = \Re(\tilde{\mathbf{u}}(\mathbf{x})e^{i\varpi t}), \quad p' = \Re(\tilde{p}(\mathbf{x})e^{i\varpi t}), \quad \eta = \Re(\tilde{\eta}(\chi)e^{i\varpi t}), \quad (4.1)$$

where $\tilde{\mathbf{u}}$, \tilde{p} and $\tilde{\eta}$ are complex. Equations (3.1) and (2.2) give

$$i\varpi\tilde{\mathbf{u}} = -\nabla\tilde{p} + \text{Oh}\nabla^2\tilde{\mathbf{u}}, \quad (4.2)$$

$$\nabla\cdot\tilde{\mathbf{u}} = 0, \quad (4.3)$$

whereas the boundary conditions (3.10), (3.3), (3.5) and (3.6) yield

$$\tilde{\mathbf{u}} = 0 \quad (4.4)$$

at the wall and

$$i\varpi\tilde{\eta} = \tilde{\mathbf{u}}\cdot\mathbf{n}, \quad (4.5)$$

$$\text{Oh}\mathbf{n}\cdot(\nabla\tilde{\mathbf{u}} + (\nabla\tilde{\mathbf{u}})^T)\cdot\mathbf{n} = \tilde{p} + \frac{1}{\bar{r}^2}\left(\frac{d^2\tilde{\eta}}{d\chi^2} + \tilde{\eta}\right) - \tilde{\mathbf{a}}\cdot\mathbf{x}, \quad (4.6)$$

$$\mathbf{n}\cdot(\nabla\tilde{\mathbf{u}} + (\nabla\tilde{\mathbf{u}})^T)\cdot\mathbf{t} = 0 \quad (4.7)$$

on the equilibrium interface. Finally, (3.9) and (3.11) imply

$$\frac{1}{\bar{r}}\frac{d\tilde{\eta}}{d\chi} \sim \pm\tilde{\eta}_{\pm}\left(\frac{\cot\bar{\theta}}{\bar{r}} - \frac{2i\varpi\text{Oh}}{\bar{\theta} - \sin\bar{\theta}\cos\bar{\theta}}\ln\left(\frac{R}{\bar{\lambda}}\right)\right), \quad (4.8)$$

$$\tilde{\eta} \rightarrow \tilde{\eta}_{\pm} \quad (4.9)$$

as $R \rightarrow 0$ and

$$\int_{-\bar{\theta}}^{\bar{\theta}} \tilde{\eta} d\chi = 0. \quad (4.10)$$

The general solution of the problem consists of the sum of (3.12), (4.1) and a combination of decaying modes. The latter contribution vanishes at large times, so after a transient phase, there remains the sum of (3.12) and (4.1). The value of C in (3.12) depends on the initial conditions and since, as noted earlier, (3.12) simply corresponds to a small time-independent displacement of the drop, it is of no great interest and we focus attention on (4.1). Note that, since $\varpi \neq 0$, (4.3)-(4.5) imply (4.10), which is thus automatically satisfied, but is nonetheless given here because it is needed later.

Writing $\tilde{\mathbf{a}} \cdot \mathbf{x} = \tilde{a}_x x + \tilde{a}_y y$, the solution of (4.2)-(4.10) can be expressed in terms of two particular cases, namely $\tilde{a}_x = 1, \tilde{a}_y = 0$ and $\tilde{a}_x = 0, \tilde{a}_y = 1$. Multiplying the first of these solutions by \tilde{a}_x , the second by \tilde{a}_y and taking the sum gives the general case. When $\tilde{a}_x = 1, \tilde{a}_y = 0$, $\tilde{\mathbf{u}}, \tilde{p}$ and $\tilde{\eta}$ are antisymmetric under reflection in the plane $x = 0$, while $\tilde{a}_x = 0, \tilde{a}_y = 1$ makes them symmetric. By symmetric $\tilde{\mathbf{u}}$, we mean that \tilde{u}_x changes sign, whereas \tilde{u}_y is unchanged by reflection. On the other hand, antisymmetric $\tilde{\mathbf{u}}$ does the opposite. Note that modes are either symmetric or antisymmetric.

As noted earlier, modes are determined by an eigenvalue problem. This problem can be obtained from (4.2)-(4.10) by setting $\tilde{\mathbf{a}} = 0$ and replacing $i\varpi$ by s . If ϖ were extended to complex values, the problem (4.2)-(4.10) with $\tilde{\mathbf{a}} \neq 0$ would lead to $\tilde{\mathbf{u}}, \tilde{p}$ and $\tilde{\eta}$ which tend to infinity as $\varpi \rightarrow -is$ (they have a pole as a function of complex ϖ), where s is any of the modal eigenvalues. In reality, ϖ is real and, thanks to viscous damping, all nonzero eigenvalues lie in $\Re(s) < 0$, so infinite response is avoided. However, if $\Re(s)$ is small, we expect the oscillation amplitudes $|\tilde{\mathbf{u}}|, |\tilde{p}|$ and $|\tilde{\eta}|$ to have a peak as a function of ϖ near $\varpi = \Im(s)$ of width comparable to $|\Re(s)|$. This expresses the usual resonant response of a lightly damped mode.

5. Small Oh

Up till now no assumption has been made concerning Oh. From here on we suppose small Oh, which is the only case for which we have developed a numerical procedure. We also suppose that $\lambda \ll \text{Oh}^{1/2}$ to avoid significant slip in the outer region. Regardless of whether Oh is small or not, (4.2) and (4.3) imply

$$\nabla^2 \tilde{p} = 0. \quad (5.1)$$

Several different asymptotic regions can be identified in the limit $\text{Oh} \rightarrow 0$. First of all there is the outer region, defined, as before, as the interior of the equilibrium drop away from the contact lines. The main aim of this section is to derive the small-Oh governing equations of

the outer region. These consist of (5.1) and boundary conditions which are derived in the following sections.

5.1 Wall and interfacial conditions

When Oh is small, we expect the flow in the outer region to have thin layers, thickness $O(Oh^{1/2})$, at the drop boundaries, inside which viscosity may be significant. Outside the layers inviscid theory applies. These layers appear in the velocity field, but not in the pressure distribution.

The analysis of the wall boundary layer in section A.2 leads to

$$\frac{\partial \tilde{p}}{\partial y} = \frac{Oh^{1/2}}{(i\varpi)^{1/2}} \frac{\partial^2 \tilde{p}}{\partial x^2} \quad y=0 \quad (5.2)$$

as the boundary condition for (5.1) at the wall, where the complex square root, $(i\varpi)^{1/2}$, should be interpreted as a principal value. (5.2) shows that $\partial \tilde{p} / \partial y = 0$ at leading order. However, the right-hand side represents viscous effects and can produce small, but significant modal damping, hence its inclusion here.

Using similar reasoning to section A.2, section A.3 analyses the flow near $r = \bar{r}$, with the result

$$\frac{\partial \tilde{p}}{\partial r} = \varpi^2 \tilde{\eta} \quad r = \bar{r}. \quad (5.3)$$

This is one of two boundary conditions on the liquid-gas interface. The other comes from (4.6). (4.3) implies $\mathbf{n} \cdot (\nabla \tilde{\mathbf{u}} + (\nabla \tilde{\mathbf{u}})^T) \cdot \mathbf{n} = -\mathbf{t} \cdot (\nabla \tilde{\mathbf{u}} + (\nabla \tilde{\mathbf{u}})^T) \cdot \mathbf{t}$. Thus, the viscous term in (4.6) is $O(Oh)$ smaller than the others. Neglecting this term,

$$\frac{1}{\bar{r}^2} \left(\frac{d^2 \tilde{\eta}}{d\chi^2} + \tilde{\eta} \right) = -\tilde{p} + \tilde{\mathbf{a}} \cdot \mathbf{x} \quad r = \bar{r} \quad (5.4)$$

is the second interfacial condition. Note that, according to (A.14), there is, in fact, no interfacial boundary layer at leading order. This is in agreement with the discussion in Batchelor (1967), section 5.14, which concludes that a thin boundary layer on a free surface does not involve significant variations of velocity across the layer, which is in contrast with layers on solid walls. The result is that there are no viscous terms in the interfacial conditions, hence no dissipation arising from the interface at the order $(Oh^{1/2})$ considered here.

5.2 Contact-line conditions

Consider the flow near one of the contact lines and, as before, let R denote distance from the contact line. As the contact line is approached, the wall boundary layer fills the flow when

$R = O(\text{Oh}^{1/2})$, a region we refer to as the transition region because viscosity, which is not significant outside the wall boundary layer in the outer region, is important throughout the flow for this and smaller values of R . All three terms in (4.2) are important in the transition region, which represents additional asymptotic structure in the small Oh limit. The unsteady term on the left-hand side greatly complicates the theoretical determination of $\tilde{\mathbf{u}}$, but fortunately, as we shall see, completion of the outer solution by matching does not require such determination of the transition-region velocity field.

Let ε be a small parameter measuring the order of magnitude of $\tilde{\mathbf{u}}$, \tilde{p} and $\tilde{\eta}$ in the outer region. Matching to the transition region requires the same orders of magnitude in that region. The unsteady and viscous terms in (4.2) are both of $O(\varepsilon)$, implying $\nabla\tilde{p} = O(\varepsilon)$. Thus,

$$\tilde{p} = \tilde{p}_\pm + O(\varepsilon \text{Oh}^{1/2}), \quad (5.5)$$

where \tilde{p}_\pm are $O(\varepsilon)$ constants, one for each contact line. The left-hand side of (4.6) is $O(\varepsilon \text{Oh}^{1/2})$. Thus, (4.6) and (5.5) yield

$$\frac{1}{\bar{r}^2} \frac{d^2 \tilde{\eta}}{d\chi^2} \sim \tilde{a}_x \bar{x}_\pm - \tilde{p}_\pm - \frac{\tilde{\eta}_\pm}{\bar{r}^2} \quad (5.6)$$

in the transition region. (5.6) agrees with the $R \rightarrow 0$ limit of (5.4). Thus, to the order we are working, the outer solution for $\tilde{\eta}$ continues to apply in the transition region, despite the velocity field being quite different. This is because the left-hand side of (4.6) is negligible.

The region $\lambda \ll R \ll \text{Oh}^{1/2}$ is described by the analysis of appendix B, leading to (4.8). Matching to the transition region is accomplished as follows. (4.8) contains the factor $\text{Oh} \ln(R/\tilde{\lambda}) = \beta + O(\text{Oh})$ when $R = O(\text{Oh}^{1/2})$, where

$$\beta = \text{Oh} \ln\left(\frac{\text{Oh}^{1/2}}{\tilde{\lambda}}\right). \quad (5.7)$$

Thus, matching (4.8) to the transition region gives

$$\frac{1}{\bar{r}} \frac{d\tilde{\eta}}{d\chi} \rightarrow \pm \tilde{\eta}_\pm \left(\frac{\cot \bar{\theta}}{\bar{r}} - \frac{2i\pi\beta}{\bar{\theta} - \sin \bar{\theta} \cos \bar{\theta}} \right) \quad (5.8)$$

as $R \rightarrow 0$ from within the transition region. As we saw above, the outer solution for $\tilde{\eta}$ continues to apply in the transition region. It follows that (5.8) should also hold for the outer region. (4.9) and (5.8) as $\chi \rightarrow \pm \bar{\theta}$ provide the contact-line conditions for the small-Oh outer problem. Note that, when $\bar{\theta} = \pi/2$, (5.8) is equivalent to the condition used to describe the contact line in Hocking (1987) and Lyubimov *et al.* (2006) (the nondimensional wetting parameter being $\pi/4\beta$). The term containing β in (5.8) provides a modification, as viewed

from the outer region, of the contact-line condition (3.8). This modification comes from $R \leq O(\text{Oh}^{1/2})$, the region near the contact line in which viscosity is significant throughout the flow. The logarithmic term in (5.7) reflects logarithmic variation of the interfacial-slope perturbation for $\lambda \ll R \ll \text{Oh}^{1/2}$, while the multiplicative factor of Oh expresses the viscous nature of the effect. β can be determined using equation (B.18) of appendix B and the function $Q_i(\bar{\theta})$ of Hocking and Rivers (1982) (c.f. Scott (2020)). Note that a pinned contact line can be obtained by formally taking infinite β , though this is not a case we will consider in what follows.

5.3 Logarithmic singularities

Equation (5.1) with the boundary conditions (5.2) at the wall, (5.3) and (5.4) on the equilibrium interface and (4.9) and (5.8) as $\chi \rightarrow \pm\bar{\theta}$ are almost sufficient to determine the solution in the outer region. However, it turns out there are weak ($O(\text{Oh}^{1/2})$) logarithmic singularities of \tilde{p} at the contact lines. The singularities reflect the presence of line sources at the contact lines in the outer-region solution. These sources are needed to compensate for the $O(\text{Oh}^{1/2})$ volume-flux deficit/excess carried by the wall boundary layer into the contact-line regions. Such logarithmic behaviour in the outer region should not be confused with the logarithm in (4.8). The outer region being essentially inviscid, a term like $\tilde{p} \propto \ln R$ represents a source/sink, whereas (4.8) describes the small regions near the contact lines in which viscosity is significant throughout. The existence of logarithmic singularities makes the outer solution nonunique and additional conditions are needed, conditions which are derived in section A.4 and which take the form

$$\int_0^{\bar{\theta}} \tilde{p}(R, \gamma) d\gamma \sim -\varpi^2 \tilde{\eta}_{\pm} R - i\varpi (i\varpi)^{1/2} \text{Oh}^{1/2} q_{\pm} \ln R \quad (5.9)$$

to within an additive constant as $R \rightarrow 0$ from the outer region, where

$$q_{\pm} = -\frac{\tilde{\eta}_{\pm}}{\sin \bar{\theta}} \quad (5.10)$$

and R, γ are the polar coordinates shown in figure A.1. (5.9) shows the weak logarithmic singularity referred to above. That the coefficient of the logarithmic term has the value given in (5.9) provides additional contact-line conditions which complete the small- Oh outer problem.

5.4 Solution procedure

The problem is treated as follows. A leading-order relation giving \tilde{p} in terms of $\tilde{\eta}$ is obtained using (5.2) and (5.9) without the $O(\text{Oh}^{1/2})$ terms. Thus, there is no logarithmic singularity and the wall condition is

$$\frac{\partial \tilde{p}}{\partial y} = 0 \quad y = 0. \quad (5.11)$$

Given $\tilde{\eta}$, (5.1), (5.3) and (5.11) determine \tilde{p} , but the other equations are not employed at this stage. If $\tilde{\eta}$ were known, this would determine \tilde{p} . However, since $\tilde{\eta}$ is not known, the result is a relation giving \tilde{p} in terms of $\tilde{\eta}$ at leading order. Using this relation to express the right-hand side of (5.2),

$$\frac{\partial \tilde{p}}{\partial y} = -i\varpi (i\varpi)^{1/2} \text{Oh}^{1/2} \Pi[\tilde{\eta}] \quad y = 0, \quad (5.12)$$

correct to $\text{Oh}^{1/2}$, where $\Pi[\tilde{\eta}]$ is a linear functional which is independent of ϖ , β and Oh . In what will henceforth be referred to as the full problem, (5.2) is replaced by (5.12) and all other equations (namely (5.1) with (5.3), (5.4), (4.9), (5.8) and (5.9)) are applied. Leaving aside \tilde{a}_x and \tilde{a}_y , the full problem has the parameters $\bar{\theta}$, ϖ , β and Oh . Viscous effects arising from the contact-line regions and wall boundary layer appear in (5.8), (5.12) and the logarithmic term of (5.9). Because the viscous terms in (5.9) and (5.12) originate from the wall boundary layer and have the same factor, $i\varpi (i\varpi)^{1/2} \text{Oh}^{1/2}$, it is convenient to adopt the designation boundary-layer term for both. On the other hand, the viscous term in (5.8) has the different factor $i\varpi\beta$ and will be referred to as a contact-line term. Note that the leading-order problem only determines \tilde{p} in terms of $\tilde{\eta}$ up to an additive constant. However, this constant disappears when the derivative on the right-hand side of (5.2) is taken.

Appendix C (supplementary material) details the mathematical analysis and numerical scheme used to implement the small- Oh problem described above. As usual, the numerical scheme involves the discretisation and consequent approximation of the continuous problem. The symmetric, $\tilde{a}_x = 0$, $\tilde{a}_y = 1$, and antisymmetric, $\tilde{a}_x = 1$, $\tilde{a}_y = 0$, components decouple and are treated separately. In either case, the results of appendix C can be expressed in the matrix form

$$\left(\Gamma_0 - \varpi^2 \Lambda_0 + i\varpi \left(\beta \Gamma_1 + (i\varpi)^{1/2} \text{Oh}^{1/2} \Xi \right) \right) U = Z, \quad (5.13)$$

where U is a column vector of complex unknowns, defined at the end of appendix C, Z is a real column vector representing wall vibration and Γ_0 , Λ_0 , Γ_1 and Ξ are real, square matrices. Z and these matrices are independent of ϖ , β and Oh , i.e. they only depend on $\bar{\theta}$. The contact-line and wall-boundary-layer contributions to the problem are apparent, respectively involving the coefficients β and $\text{Oh}^{1/2}$. (5.13) can be solved using a standard routine (we used LAPACK's ZGESV). This determines the drop response to wall vibration.

6. Comparison with DNS

The DNS results with which the theory is compared were obtained as follows. The basis of the simulations is the same as that of the theory, in particular the frame of reference of the wall is used, as are the Navier-Stokes equations, (2.1) and (2.2), and the wall boundary condition (2.4). An important difference is that DNS retains nonlinearity, whereas the theory does not. As in the theory, the wall vibration is sinusoidal. Vibrations are perpendicular to the wall (i.e. $\tilde{a}_x = 0$) for the simulations whose results are presented here. This allows a symmetric flow and, using this assumption, DNS was restricted to $x \geq 0$.

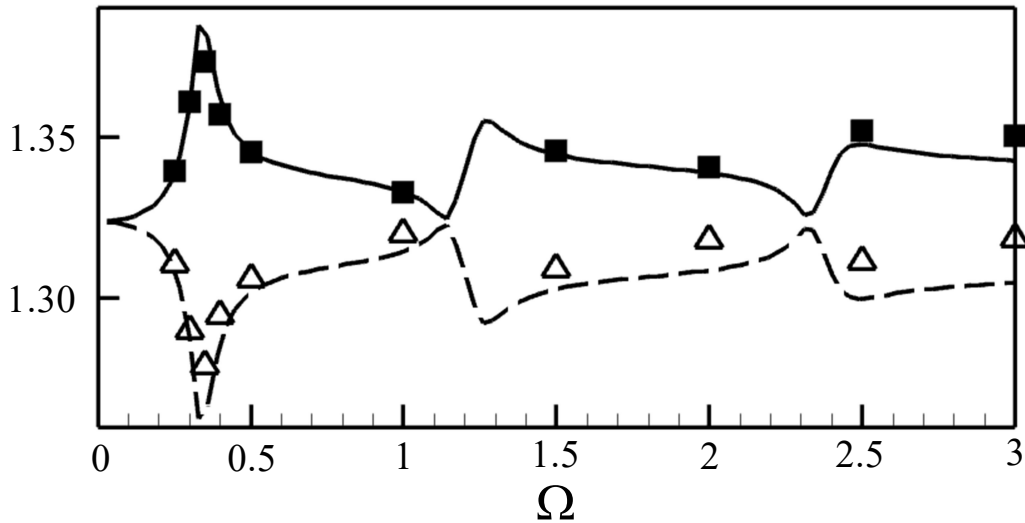


Figure 2: Minimum and maximum contact-line values of x as a function of $\Omega = \omega / 2\pi$. The symbols are DNS results.

The DNS code is two-dimensional and based on the Two-Phase Level-Set (TPLS) method (O’Naraigh *et al.*, 2014). The advection equation of the level-set function, which is the signed distance to the interface, is solved in a conservative way using a third-order Total-Variation-Diminishing Runge Kutta (TVD RK3) time discretization scheme (Osher and Shu, 1988) and a fifth-order Weighted-Essentially-Non-Oscillatory (WENO5) scheme (Jiang and Shu, 1996) for the reconstruction of the level-set function at the cell boundaries of the staggered computational grid. Redistancing is then carried out by solving a Hamilton-Jacobi equation in pseudo-time to enforce $|\nabla\varphi|=1$ (Sussman *et al.*, 1994), φ being the level-set function. This is done using a WENO5 scheme for first derivatives, with divided differences in the vertical direction set to $-\cos\bar{\theta}$ at the wall and a TVD RK2 scheme for integration in pseudo-time, along with the method suggested by Sussman and Fatemi (1999) to improve local volumetric conservation - the result is the SF-W5-RK2 method of Solomenko *et al.* (2017a), which was also used in Solomenko *et al.* (2017b). In the latter article, the flow was not resolved down to the slip length and thus a subgrid model was used near the contact lines. Here, however, the slip region is fully resolved so subgrid modelling is not needed. After redistancing, the method of Sussman and Uto (1998) is used to enforce exact volumetric conservation. The wall boundary condition, (2.4), is applied as in Afkhami *et al.* (2009). A symmetry condition

is used on the boundary $x=0$, while outflow conditions are applied on the remaining boundaries, i.e. at the top and right-hand side of the computational domain.

Because DNS incurs a huge computational cost, only a single set of the parameters $\bar{\theta}$, λ and Oh was treated, namely $\bar{\theta} = \pi/4$, $\lambda = \text{Oh} = 5 \times 10^{-3}$, as well as a limited number of ϖ . Whereas the theory is linear, DNS allows for nonlinearity, so a potentially significant additional parameter is the displacement amplitude, A , of the wall, which gives the wall acceleration amplitudes $\tilde{a}_x = 0$, $\tilde{a}_y = -\varpi^2 A$. $A = 0.025$ for the results given here. Figures 2-4 provide a comparison of the DNS results and those of the present theory, obtained by solving (5.13). The DNS results are taken following the transient phase in which the drop response is not yet periodic, a phase discussed earlier in the linearized context. The equilibrium contact-line position and drop height are $\bar{x}_+ = 1.3236$ and 0.54826 for the given $\bar{\theta} = \pi/4$. Figure 2 shows the minimum and maximum contact-line values of x as a function of $\Omega = \varpi/2\pi$. The curves give theoretical results, while the symbols follow from DNS. Figure 3 is the equivalent for the drop height. Figure 4 shows the phase of oscillation of the drop height and contact-line position. There is good agreement between DNS and theory in figures 2 and 3 at

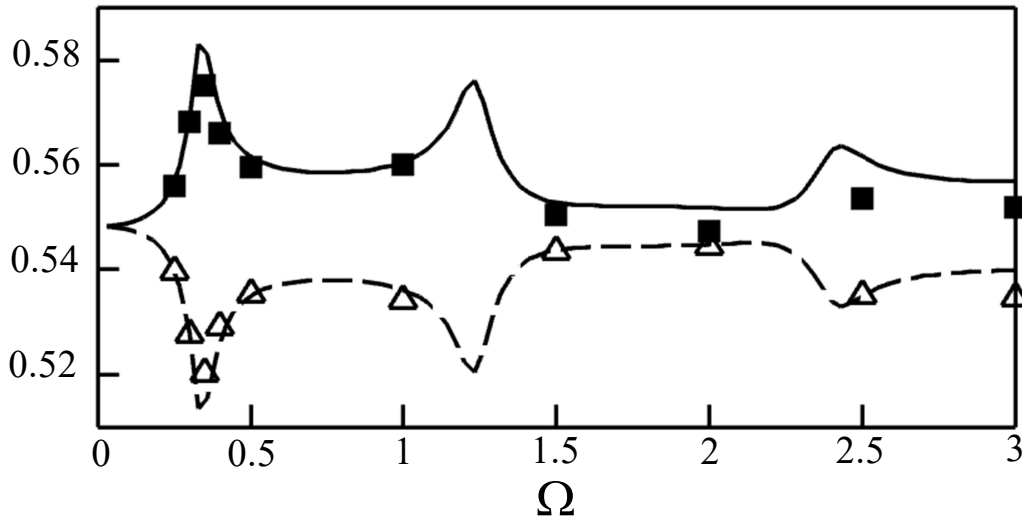


Figure 3: Minimum and maximum drop height as a function of $\Omega = \varpi/2\pi$. The symbols are DNS results.

lower values of Ω , but the agreement is less good towards the right-hand sides of these figures. This seems to be due to increasing effects of nonlinearity. This is apparent in the figures because linear theory leads to the minimum and maximum of any oscillating quantity being symmetrically placed about its equilibrium value, which is not so towards the right-hand sides of figures 2 and 3. On the other hand, the phases shown in figure 4 appear to be less affected. Of course, nonlinearity increases in importance as A increases and accord with linear theory is only to be expected at small A . Note that, as $\varpi \rightarrow 0$, the drop-height oscillations are in phase with those of the wall, whereas the contact-line oscillations are in antiphase.

The overall conclusion is that there is good agreement between DNS and theory, the differences being probably due to nonlinearity at higher frequencies. This lends confidence in both the DNS and the semi-analytical model developed here.

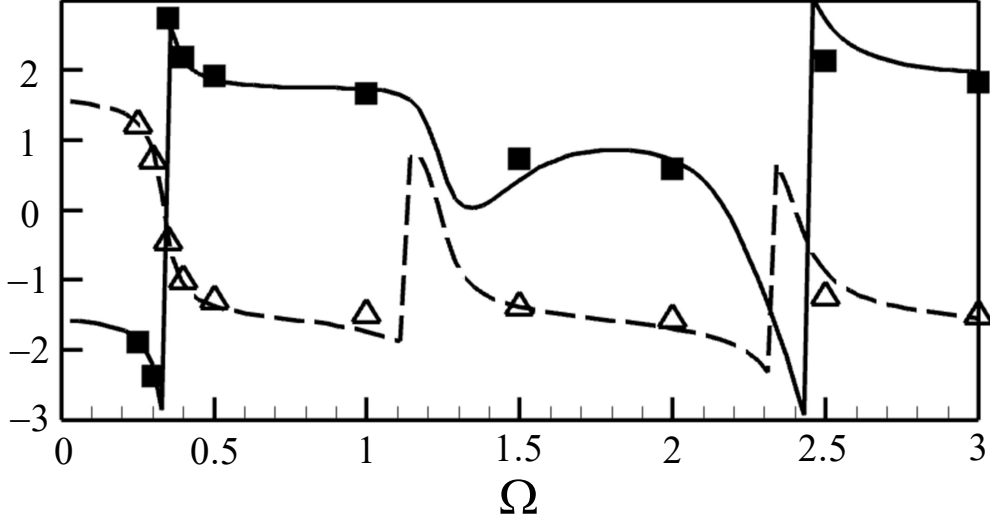


Figure 4: Phase of oscillation of the drop height (squares and continuous curve) and contact-line position (triangles and dashed curve) as a function of $\Omega = \varpi / 2\pi$. The symbols are DNS results. The phase of the wall-displacement oscillation is $-\pi/2$.

7. Lightly damped modes near resonance

This section uses (5.13) to analyse the resonant response of lightly damped modes. In the inviscid case, $\beta = \text{Oh} = 0$, modes result from the generalised eigenvalue problem

$$(\Gamma_0 - \lambda \Lambda_0)U = 0, \quad (7.1)$$

which we solved using LAPACK's DGGEV (the eigenvalue λ should not be confused with the slip length). As expected, there are purely oscillatory modes, corresponding to $\lambda = \omega^2$ real and positive, where ω is the modal frequency. In the antisymmetric case, there is a mode very close to $\lambda = 0$. This is a numerical approximation of the steady mode, discussed earlier, which represents a time-independent displacement of the drop and for which $\lambda = 0$, $\mathbf{u} = 0$, $p' = 0$ and $\eta = C \sin \chi$. As is usual for generalised eigenvalue problems, there are infinite eigenvalues defined by $\Lambda_0 U = 0$. We also found modes with large, finite, complex and negative real values of λ . These are presumably spurious and due to numerical approximation of the eigenvalue problem. Let us denote the finite eigenvalues by λ_α and the corresponding eigenvectors by U_α . Thus,

$$(\Gamma_0 - \lambda_\alpha \Lambda_0)U_\alpha = 0. \quad (7.2)$$

The U_α are often referred to as right eigenvectors, whereas for each λ_α there is also a left eigenvector, $U_{\alpha,L}$, such that

$$U_{\alpha,L}^H (\Gamma_0 - \lambda_\alpha \Lambda_0) = 0, \quad (7.3)$$

where H denotes Hermitian conjugation. The left and right eigenvectors are orthogonal in the sense that

$$U_{\alpha,L}^H \Lambda_0 U_{\alpha'} = 0 \quad (7.4)$$

for $\alpha' \neq \alpha$.

Let us first consider the symmetric problem. Left-multiplying (5.13) by $U_{\alpha,L}^H$ and using (7.3),

$$U_{\alpha,L}^H \left((\lambda_\alpha - \varpi^2) \Lambda_0 + i\varpi \left(\beta \Gamma_1 + (i\varpi)^{1/2} \text{Oh}^{1/2} \Xi \right) \right) U = U_{\alpha,L}^H Z. \quad (7.5)$$

Assuming the eigenvectors form a complete set, we write

$$U = U_\infty + \sum_{\alpha'} C_{\alpha'} U_{\alpha'}, \quad (7.6)$$

where U_∞ is the contribution from infinite eigenvalues. Using $\Lambda_0 U_\infty = 0$ and (7.4),

$$U_{\alpha,L}^H \Lambda_0 U_\alpha (\lambda_\alpha - \varpi^2) C_\alpha + i\varpi U_{\alpha,L}^H \left(\beta \Gamma_1 + (i\varpi)^{1/2} \text{Oh}^{1/2} \Xi \right) U = U_{\alpha,L}^H Z. \quad (7.7)$$

Consider a mode with real, positive λ_α . Assuming the mode is lightly damped when viscous effects are included and that ϖ is close to the resonance condition $\varpi^2 = \omega_\alpha^2$, where $\omega_\alpha = \lambda_\alpha^{1/2} > 0$, we expect the dominant contribution to (7.6) to come from $\alpha' = \alpha$. Neglecting the other terms yields the approximation

$$U = C_\alpha U_\alpha, \quad (7.8)$$

hence (7.7) gives

$$C_\alpha = \frac{B^\alpha}{\varpi^2 - \omega_\alpha^2 - 2i\varpi \left(\beta D_c^\alpha + (i\varpi)^{1/2} \text{Oh}^{1/2} D_w^\alpha \right)}, \quad (7.9)$$

where

$$B^\alpha = -\frac{U_{\alpha,L}^H Z}{U_{\alpha,L}^H \Lambda_0 U_\alpha}, \quad (7.10)$$

$$D_c^\alpha = \frac{U_{\alpha,L}^H \Gamma_1 U_\alpha}{2U_{\alpha,L}^H \Lambda_0 U_\alpha}, \quad D_w^\alpha = \frac{U_{\alpha,L}^H \Xi U_\alpha}{2U_{\alpha,L}^H \Lambda_0 U_\alpha}. \quad (7.11)$$

(7.8)-(7.11) determine U for a lightly damped mode close to resonance. Because λ_α is real, the eigenvectors U_α and $U_{\alpha,L}$ can be chosen real. Thus, the quantities B^α , D_c^α and D_w^α are real and only depend on $\bar{\theta}$ and the choice of mode. D_c^α and D_w^α represent viscous effects due to the contact lines and wall boundary layer.

Let $\varpi > 0$. Because ϖ is close to ω_α , $\varpi^2 - \omega_\alpha^2$ can be approximated by $2\omega_\alpha(\varpi - \omega_\alpha)$ and ϖ by ω_α in the viscous terms of (7.9), leading to

$$C_\alpha = \frac{B^\alpha}{2\omega_\alpha(\varpi - \omega_\alpha - iD^\alpha)}, \quad (7.12)$$

where $D^\alpha = D_r^\alpha + iD_i^\alpha$,

$$D_r^\alpha = \beta D_c^\alpha + \text{Oh}^{1/2} \hat{D}_w^\alpha, \quad D_i^\alpha = \text{Oh}^{1/2} \hat{D}_w^\alpha, \quad (7.13)$$

and $\hat{D}_w^\alpha = 2^{-1/2} \omega_\alpha^{1/2} D_w^\alpha$. (7.12) has the expected form for the complex amplitude of a lightly-damped mode near resonance. It implies that the effect of viscosity is to perturb the complex modal frequency from its inviscid value, ω_α , to become $\omega_\alpha + iD^\alpha$. Given the modal time-dependence, $e^{i\omega t}$, D_r^α is a damping factor and $-D_i^\alpha$ a shift in modal frequency. The modal amplitude, $|C_\alpha|$, has a maximum at the shifted frequency $\varpi = \omega_\alpha - D_i^\alpha$ according to (7.12). The first of equations (7.13) expresses the damping as a sum of contact-line and wall-boundary-layer contributions, βD_c^α and $\text{Oh}^{1/2} \hat{D}_w^\alpha$, whereas the second indicates that the frequency shift arises from the boundary layer. Because the contact lines and boundary layer should both induce damping, we expect positive D_c^α and \hat{D}_w^α and this is found to be the case. Positive \hat{D}_w^α implies a modal frequency lower than its inviscid value. The condition of light damping used to derive the above results requires that D_r^α be small, which in turn implies a small modal frequency shift. The relative importance of boundary-layer and contact-line damping is measured by the ratio,

$$\rho_\alpha = \nu_\alpha \frac{\text{Oh}^{1/2}}{\beta}, \quad (7.14)$$

of their damping factors, where $\nu_\alpha = \hat{D}_w^\alpha / D_c^\alpha$.

Turning attention to the antisymmetric case, the inviscid solution of the vibration problem with $\tilde{a}_x = 1$, $\tilde{a}_y = 0$ is $\tilde{u}_x = i\varpi^{-1}$, $\tilde{u}_y = 0$, $\tilde{p} = x$, $\tilde{\eta} = \varpi^{-2} \sin \chi$. This represents oscillation of the equilibrium drop parallel to the wall with displacement amplitude ϖ^{-2} , oscillation which is simply due to use of the wall's frame of reference. In the inviscid drop's frame of reference, which is inertial, the equilibrium is unperturbed. This is because, in the absence of viscosity, the drop has no means of sensing tangential wall motion. Denoting the inviscid

solution by $U = \varpi^{-2}V$, V is a constant, real column vector whose components are explicitly given at the end of appendix C and which satisfies

$$\Gamma_0 V = 0, \quad \Lambda_0 V = -Z. \quad (7.15)$$

Thus, (5.13) implies

$$\left(\Gamma_0 - \varpi^2 \Lambda_0 + i\varpi \left(\beta \Gamma_1 + (i\varpi)^{1/2} \text{Oh}^{1/2} \Xi \right) \right) W = Z_a, \quad (7.16)$$

where $W = U - \varpi^{-2}V$ and

$$Z_a = -i\varpi^{-1} \left(\beta \Gamma_1 + (i\varpi)^{1/2} \text{Oh}^{1/2} \Xi \right) V. \quad (7.17)$$

Treating (7.16) as we did (5.13) for the symmetric problem,

$$W = W_\infty + \sum_{\alpha'} C_\alpha U_{\alpha'}, \quad (7.18)$$

$$U_{\alpha,L}^H \Lambda_0 U_\alpha (\lambda_\alpha - \varpi^2) C_\alpha + i\varpi U_{\alpha,L}^H \left(\beta \Gamma_1 + (i\varpi)^{1/2} \text{Oh}^{1/2} \Xi \right) W = U_{\alpha,L}^H Z_a. \quad (7.19)$$

Let α be a mode, other than the one with very small λ_α , having real, positive λ_α . For a lightly damped mode near resonance, we argue, as in the symmetric case, that (7.18) is dominated by $\alpha' = \alpha$, leading to

$$C_\alpha = \frac{i\varpi^{-1} \left(\beta B_c^\alpha + (i\varpi)^{1/2} \text{Oh}^{1/2} B_w^\alpha \right)}{\varpi^2 - \omega_\alpha^2 - 2i\varpi \left(\beta D_c^\alpha + (i\varpi)^{1/2} \text{Oh}^{1/2} D_w^\alpha \right)}, \quad (7.20)$$

where (7.17) has been used, D_c^α and D_w^α are given by (7.11) and

$$B_c^\alpha = \frac{U_{\alpha,L}^H \Gamma_1 V}{U_{\alpha,L}^H \Lambda_0 U_\alpha}, \quad B_w^\alpha = \frac{U_{\alpha,L}^H \Xi V}{U_{\alpha,L}^H \Lambda_0 U_\alpha}. \quad (7.21)$$

As for the symmetric case, D_c^α and D_w^α are real and only depend on $\bar{\theta}$ and the choice of mode. The same is true of B_c^α and B_w^α . Given $W = U - \varpi^{-2}V$ and dominance of the $\alpha' = \alpha$ term in (7.18),

$$U = \varpi^{-2}V + C_\alpha U_\alpha \quad (7.22)$$

which, with (7.11), (7.20) and (7.21), gives U in the antisymmetric case. It consists of a term, $C_\alpha U_\alpha$, which involves resonance and an inviscid one, $\varpi^{-2}V$, which does not. The latter disappears when the results are transferred to the inertial frame of reference of the inviscid drop. Note that (7.20) gives $C_\alpha = 0$ in the inviscid case, reflecting the ineffectiveness

of tangential wall vibration on the drop in the absence of viscosity. This contrasts with the symmetric case.

When $\varpi > 0$, ϖ is close to $\omega_\alpha = \lambda_\alpha^{1/2}$ and (7.20) can be further approximated as

$$C_\alpha = \frac{i\left(\beta B_c^\alpha + (i\omega_\alpha)^{1/2} \text{Oh}^{1/2} B_w^\alpha\right)}{2\omega_\alpha^2\left(\varpi - \omega_\alpha - iD^\alpha\right)}, \quad (7.23)$$

where $D^\alpha = D_r^\alpha + iD_i^\alpha$ and (7.13) holds. The discussion following that equation applies as before.

Finally, consider the mode α with very small λ_α . Supposing it is lightly damped, we expect this mode to dominate the sum in (7.18) at small ϖ . Thus, (7.20) holds, as for the modes away from $\omega_\alpha = 0$. In the absence of numerical approximation of the inviscid eigenvalue problem, $\omega_\alpha = 0$ for the given mode. Thus, we set $\omega_\alpha = 0$ in (7.20) to obtain

$$C_\alpha = \frac{i\left(\beta B_c^\alpha + (i\varpi)^{1/2} \text{Oh}^{1/2} B_w^\alpha\right)}{\varpi^2\left(\varpi - 2i\left(\beta D_c^\alpha + (i\varpi)^{1/2} \text{Oh}^{1/2} D_w^\alpha\right)\right)}, \quad (7.24)$$

where (7.11) and (7.21) apply as before. The light-damping assumption of this mode requires small βD_c^α and $\text{Oh}^{1/2} D_w^\alpha$.

8. Results

Here we give some results of the semi-analytic model. Section 8.1 concerns the variation of the inviscid modal frequencies as a function of contact angle. These frequencies form an important foundation for interpretation of the response to wall vibration because they determine the approximate location of the resonant peaks as a function of frequency when the modes are lightly damped. Section 8.2 gives an illustrative example of the response to vibration. Finally, section 8.3 quantifies the modal damping coefficients D_c^α and \hat{D}_w^α as functions of $\bar{\theta}$. As discussed in section 7, these coefficients control the viscous damping and frequency shift for lightly damped modes. The damping in turn determines the magnitude of the resonant response and the width of the resonant peak. The relative importance of the boundary-layer and contact-line contributions to damping is quantified.

The numerical procedure used to implement the model and described in appendix C involves truncation of certain infinite series. The number of retained terms was chosen sufficiently large that the accuracy of the sums was close to machine precision (IEEE double precision was used throughout). The procedure also involves the numerical parameters τ_M and Δ , of which τ_M should be large and Δ small. Varying both and comparing results for different choices, we found that $\tau_M = 10$ and $\Delta = 0.01$ lead to convergence such that the

differences between the numerical and exact solutions are much lower than would be visible in most of the plots given here (figure 5 near $\bar{\theta} = \pi$ being the exception). These values of τ_M and Δ are used in what follows (and were also used when calculating the theoretical values for figures 2-4).

8.1 Inviscid-mode frequencies

For comparison with later results with the wall, the inviscid modes of a 2D drop without a wall have nondimensional frequencies determined by $\omega^2 = \pi^{3/2}n(n^2 - 1)$, where n is a positive integer. As an illustration, $n = 8$ gives $\omega = 52.976$.

Figure 5 shows the first eight symmetric and antisymmetric inviscid, nonzero modal frequencies, obtained by solution of (7.1), as a function of $\bar{\theta}$. The continuous curves represent the symmetric case, whereas the dashed ones correspond to the antisymmetric one.

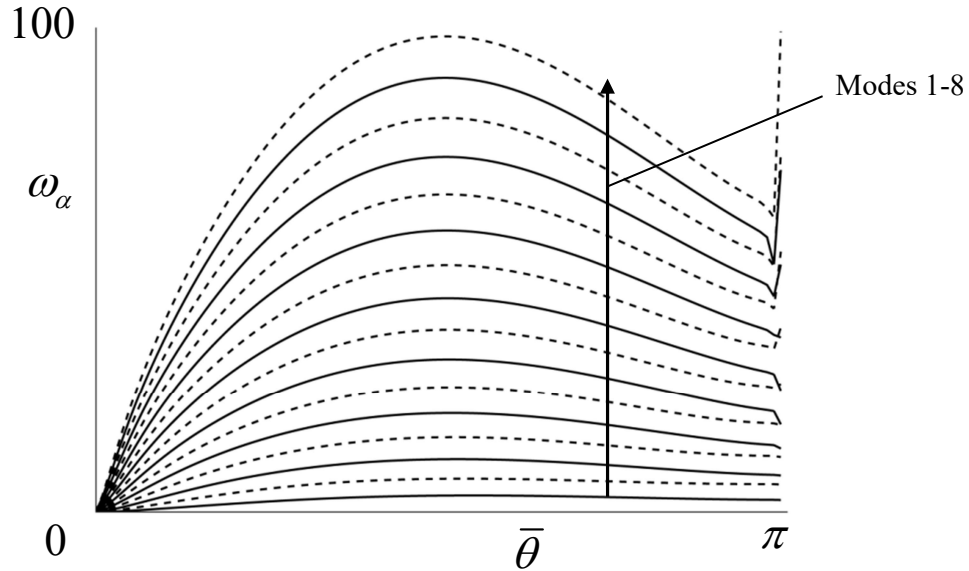


Figure 5: Inviscid modal frequencies as a function of $\bar{\theta}$. The solid curves are the symmetric modes, whereas the dashed curves are the antisymmetric ones.

A numerical problem is evident near $\bar{\theta} = \pi$, a problem which arises because the bipolar coordinate system used in appendix C is not appropriate there. This is because the discretisation of the equilibrium liquid/gas interface places more and more points near $x = y = 0$ in this limit, whereas it continues to extend to $x, y = O(1)$. Thus, most of the interface is not covered. Leaving this region aside, frequencies alternate between symmetric and antisymmetric modes for a given $\bar{\theta}$, the lowest nonzero frequency being for a symmetric mode. For each mode, $\omega_\alpha(\bar{\theta})$ has a maximum. This occurs at $\bar{\theta} = 1.714$ for the lowest

frequency (symmetric) mode, an angle which decreases as the modal order is increased and appears to approach the limit $\pi/2$ at large order. This can be understood as follows. High-order modes consist of short wavelength capillary waves on the liquid/gas interface. Being of short wavelength, the equilibrium interface can be approximated as flat. For capillary waves on a flat interface, the dispersion relation is $\omega = |k|^{3/2}$, where k is the wavenumber. Waves propagate in both directions along the interface and undergo reflection at the contact lines, thus forming a standing wave, which is the mode. Let n denote the modal order. At large n we expect $\sim n$ half-wavelengths along the interface, i.e. $|k| \sim n\pi/\ell$, where ℓ is the interfacial length. Since $\ell = 2\bar{\theta}\bar{r}$ and $\bar{r} = (\bar{\theta} - \sin\bar{\theta}\cos\bar{\theta})^{-1/2}$,

$$\omega \sim \left(\frac{1}{2} n\pi \frac{(\bar{\theta} - \sin\bar{\theta}\cos\bar{\theta})^{1/2}}{\bar{\theta}} \right)^{3/2}, \quad (8.1)$$

which has a maximum at $\bar{\theta} = \pi/2$.

The inviscid modes can be determined analytically when $\bar{\theta} = \pi/2$. They have $\omega^2 = n(n^2 - 1)\bar{r}^{-3}$, $\tilde{p} = (n^2 - 1)\bar{r}^{-n-2}r^n \cos n(\chi - \pi/2)$ and $\tilde{\eta} = \cos n(\chi - \pi/2)$, where n is a positive integer and $\bar{r} = (2/\pi)^{1/2}$. Even and odd n correspond respectively to symmetric and antisymmetric modes. The zero frequency antisymmetric mode discussed earlier has $n = 1$.

The behaviour of the inviscid, nonzero modal frequencies near $\bar{\theta} = \pi$ can be determined by asymptotic analysis. It is found that the first ten symmetric and antisymmetric frequencies approach the values given in table 1 as $\bar{\theta} \rightarrow \pi$. This indicates how figure 5 would go as $\bar{\theta} \rightarrow \pi$ in the absence of the numerical problem. The antisymmetric frequencies for $\bar{\theta} = \pi$ have the values $\omega^2 = \pi^{3/2}n(n^2 - 1)$, where n is a positive integer, as for a 2D drop without the wall. The value of n runs from 2 to 11 in table 1.

Symmetric	Antisymmetric
2.573148	5.780136
7.659789	11.56027
13.73370	18.27839
20.73436	25.84955
28.56548	34.19574
37.15165	43.25457
46.43382	52.97582
56.36453	63.31821
66.90468	74.24719
78.02141	85.73327

Table 1: Values of the $\bar{\theta} = \pi$ inviscid modal frequencies.

8.2 Illustrations of the response to vibration

The solid curves in figures 6 and 7 show the calculated response to vibration with $\tilde{a}_x = 0$, $\tilde{a}_y = -\varpi^2 A$, for $\bar{\theta} = \pi/3$, $\lambda = \text{Oh} = 5 \times 10^{-3}$ (which lead to $\beta = 0.013956$). Figure 6 shows the contact-line displacement amplitude divided by the wall displacement amplitude, i.e. $|\tilde{\eta}_- / A| / \sin \bar{\theta}$, as a function of ϖ . Figure 7 shows $|\tilde{\eta}(\chi = 0) / A|$, which represents the drop-height amplitude as a multiple of the wall amplitude. The peaks in both figures are close to the inviscid modal frequencies, represented by the vertical dashed lines. Thus, the peaks are the consequence of resonances. The relative importance of contact-line and boundary-layer damping, as measured by ρ_α (given by (7.14)), has values which decrease with increasing modal frequency from 1.15 for the first mode to 0.648 for the fifth. Thus, the two damping mechanisms are here of comparable importance. The dashed curves indicate the results of using the approximation (7.8) and (7.9), which, it will be recalled, should hold for lightly damped modes near resonance. Both the locations and heights of the peaks are reasonably well represented, in particular for the first mode, which is more lightly damped than the others. Note that figure 6 indicates frequencies at which the contact-line oscillation amplitude is nearly zero. In the inviscid case, the solution of (5.13) is real, which suggests the possibility that there are exact zeroes of the contact-line amplitude as a function of ϖ and this is found to be the case. That there are near zeroes in the slightly viscous problem is thus not unreasonable. Note however that, according to figure 7, the height amplitude does not exhibit such near zeroes.

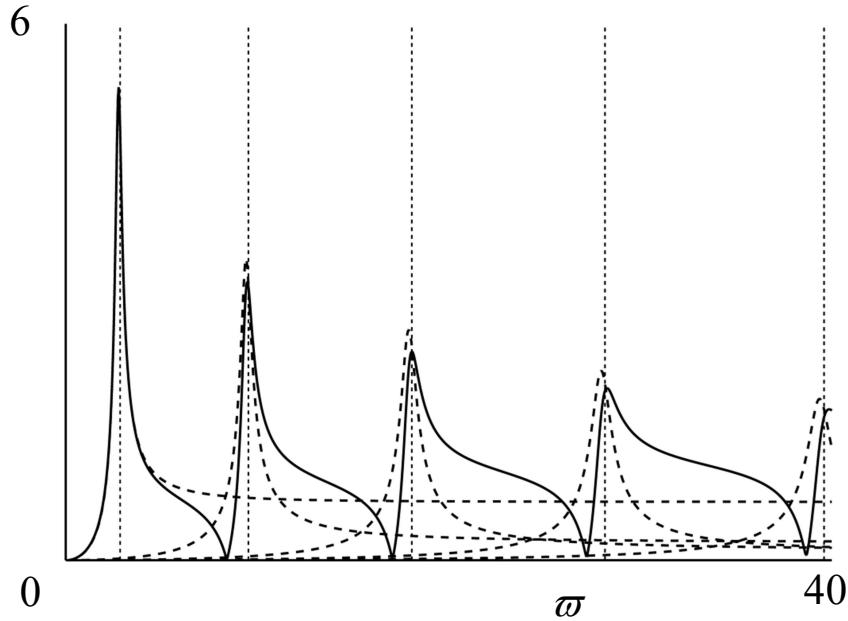


Figure 6: Solid curve: contact-line displacement amplitude, $|\tilde{\eta}_- / A| / \sin \bar{\theta}$, as a function of ϖ ($\bar{\theta} = \pi/3$, $\lambda = \text{Oh} = 5 \times 10^{-3}$) for the symmetric problem. Dashed curves: results of (7.8), (7.9) for each of the first five modes. Vertical dashed lines: inviscid modal frequencies.

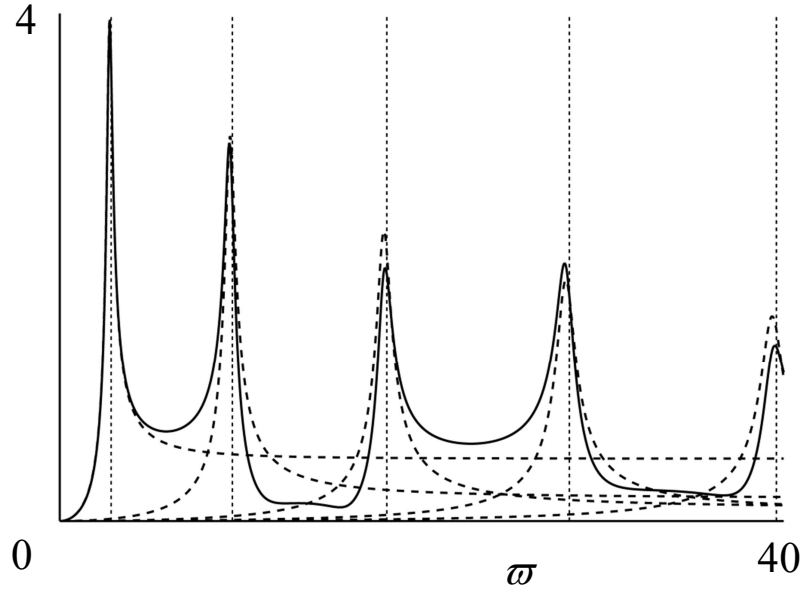


Figure 7: Solid curve: drop-height oscillation amplitude, $|\tilde{\eta}(\chi=0)/A|$, as a function of ϖ ($\bar{\theta} = \pi/3$, $\lambda = \text{Oh} = 5 \times 10^{-3}$) for the symmetric problem. Dashed curves: results of (7.8), (7.9) for each of the first five modes. Vertical dashed lines: inviscid modal frequencies.

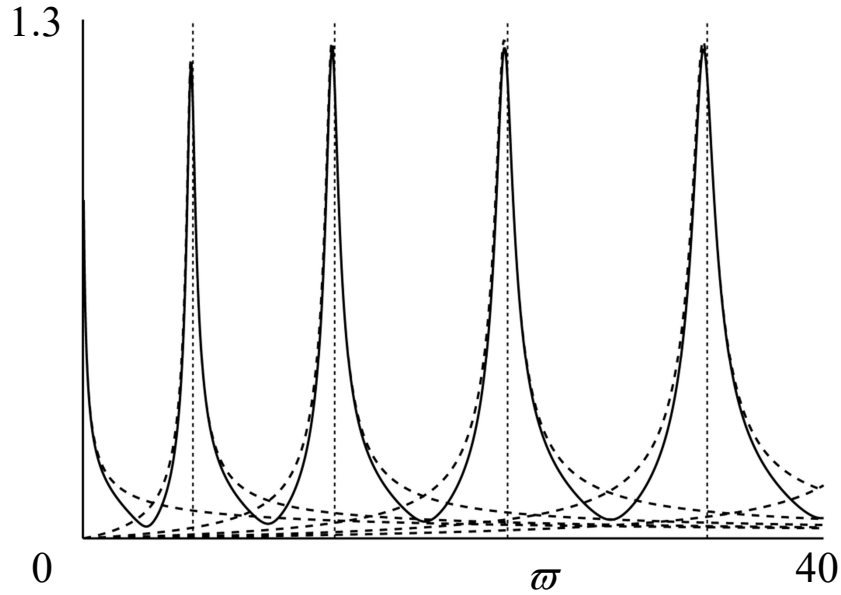


Figure 8: Solid curve: contact-line displacement amplitude in the inertial frame of reference of the inviscid drop, $|1 - A^{-1}\tilde{\eta}_-/\sin\bar{\theta}|$, as a function of ϖ ($\bar{\theta} = \pi/3$, $\lambda = \text{Oh} = 5 \times 10^{-3}$) for the antisymmetric problem. Dashed curves: results of (7.22) (without the term in V) with (7.20) for each of the first five oscillatory modes and (7.24) for the zero frequency one. Vertical dashed lines: inviscid modal frequencies.

Figure 8 is the equivalent of figure 6, but for the antisymmetric case, $\tilde{a}_x = -\varpi^2 A$, $\tilde{a}_y = 0$. Note that it is $|1 - A^{-1}\tilde{\eta}_-/\sin\bar{\theta}|$ which is plotted in figure 8. This is the contact-line displacement amplitude in the inertial frame of reference of the inviscid drop, divided by the wall displacement amplitude. There are once again resonant peaks near the inviscid modal frequencies. The dashed curves represent the approximation (7.22) (without the term in V , the frame of reference being that of the inviscid drop) with (7.20), (7.24) and express the behaviour near $\varpi = 0$ and the resonant peaks well. For modes other than the zero frequency one, ρ_α decreases with increasing modal frequency from 0.969 for the first mode to 0.668 for the fourth. Thus, contact-line and boundary-layer damping are of comparable importance, as for the symmetric case.

8.3 Measures of damping

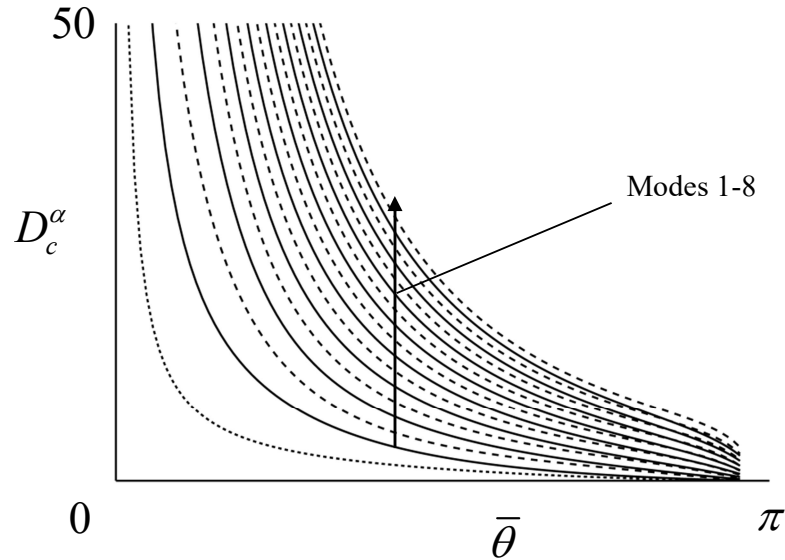


Figure 9: Contact-line damping coefficients for the first eight symmetric (solid curves) and antisymmetric (dashed curves) modes. The finely dashed curve is for the zero-frequency antisymmetric mode.

Figures 9 and 10 show D_c^α and \hat{D}_w^α as functions of $\bar{\theta}$ for the first eight oscillatory symmetric and antisymmetric modes. For completeness sake, they also show results for the zero-frequency antisymmetric mode. However, we focus on the other modes in what follows. To avoid the numerical problems noted earlier and apparent in figure 5, the maximum $\bar{\theta}$ for these plots is 3. Numerical problems are also responsible for the absence of a small range of $\bar{\theta}$ on the left of figure 10. As indicated by the arrow in both figures, symmetric modes of increasing inviscid frequency give increasing values of D_c^α and \hat{D}_w^α , as do antisymmetric modes. Recalling from the first of equations (7.13) that the damping factor for lightly-

damped modes is the sum of contact-line and boundary-layer contributions, βD_c^α and $\text{Oh}^{1/2} \hat{D}_w^\alpha$, it can be obtained by multiplying the value from figure 9 by β , that from figure 10 by $\text{Oh}^{1/2}$ and summing. Both damping contributions should be small compared with the separation between successive inviscid modal frequencies for damping to be light, otherwise sharp resonant response is not expected. From figure 9, it is apparent that light damping requires smaller and smaller β as $\bar{\theta}$ decreases, particularly for higher modes. This is especially true because the separation between mode frequencies is smaller at lower $\bar{\theta}$, as is apparent from figure 5. Similarly, figure 10 indicates that it is harder to achieve light boundary-layer damping for higher modes and lower $\bar{\theta}$, requiring smaller values of $\text{Oh}^{1/2}$.

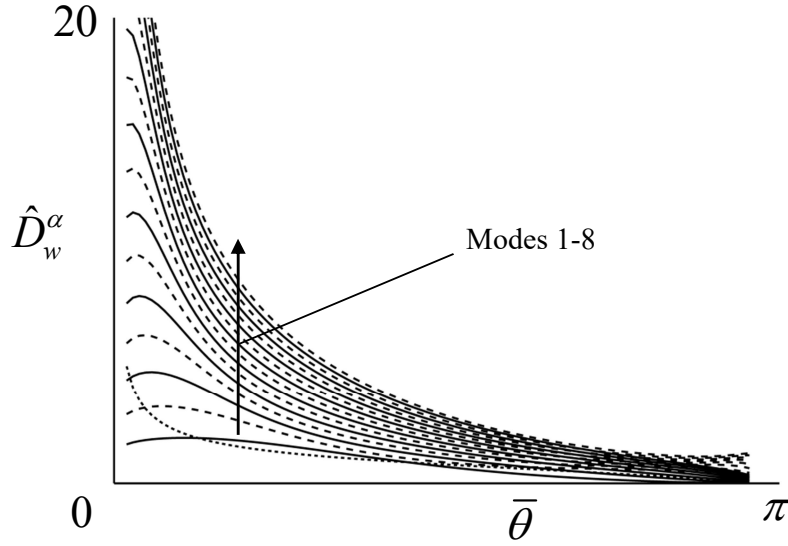


Figure 10: Boundary-layer damping coefficients for the first eight symmetric (solid curves) and antisymmetric (dashed curves) modes. The finely dashed curve represents D_w^α (not \hat{D}_w^α , which would be zero) for the zero-frequency antisymmetric mode.

Figure 11 shows $\nu_\alpha = \hat{D}_w^\alpha / D_c^\alpha$ as a function of $\bar{\theta}$ for the first eight oscillatory symmetric and antisymmetric modes. Apart from the first symmetric mode towards the right-hand side of the figure (and probably higher-order symmetric modes closer to $\bar{\theta} = \pi$), ν_α decreases as the mode frequency increases for a given $\bar{\theta}$. According to (7.14), when ν_α is multiplied by $\text{Oh}^{1/2} / \beta$, the result measures the relative importance of boundary-layer and contact-line damping for lightly damped modes. Thus, if $\beta / \text{Oh}^{1/2}$ is comparable with ν_α the two damping mechanisms are of similar importance. On the other hand, when $\beta / \text{Oh}^{1/2}$ is small or large compared to ν_α one of the two mechanisms dominates. It appears that contact-line damping is favoured at smaller values of $\bar{\theta}$, while, in the antisymmetric case, boundary-layer damping tends to be more important at larger contact angles and higher modes. Of course, for a given contact angle and mode, the relative importance of the two damping mechanisms

depends on the value of $\beta/Oh^{1/2}$. Cases can be found in which these mechanisms are comparable, as was the case for the parameter values used in figures 6-8, or one or the other dominates.

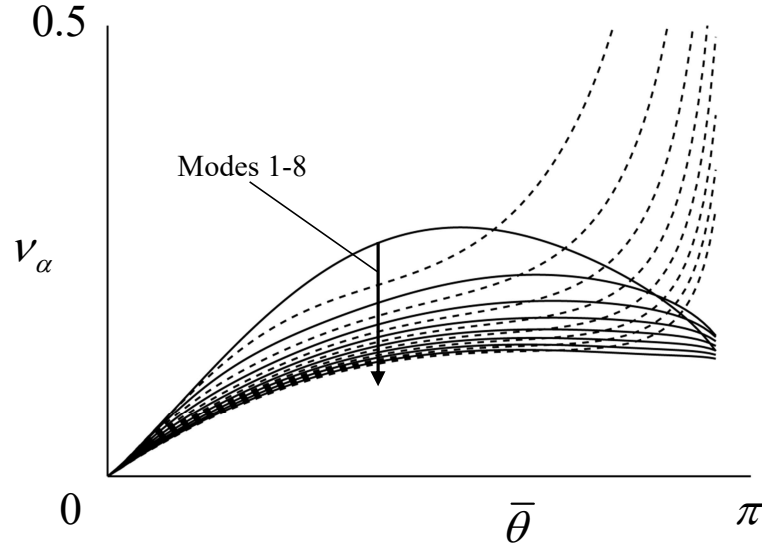


Figure 11: Ratio of boundary-layer to contact-line damping coefficients for the first eight symmetric (solid curves) and antisymmetric (dashed curves) modes.

9. Conclusions

A linearized model of a two-dimensional liquid drop surrounded by gas on a vibrating wall has been developed. The moving contact lines are allowed for using a Navier-type boundary condition at the wall, which introduces a slip length λ , and a prescribed angle of intersection of the liquid/gas interface with the wall. In the absence of vibration, the drop has an equilibrium state in which the interface is circular. Small vibration perturbs this state and the governing equations of the perturbation are linearized. Wall vibration can have both normal and tangential components. In the linear problem, these can be analysed separately and the results summed to produce the overall response. Normal vibration produces a symmetric drop motion, whereas it is antisymmetric for tangential vibration.

When λ is small, as expected in practice, the drop can be separated into an outer region, away from the contact lines, and regions near the contact lines whose analysis is described in appendix B. This leads to conditions for the outer problem as the distance, R , to one of the contact lines tends to zero. The result completes the outer problem.

Specialising to sinusoidal wall motion with frequency $\varpi \neq 0$, the drop response consists of a time-independent displacement, (3.12), a sum of exponentially decaying, oscillatory normal modes and a sinusoidal component, which is given by (4.1). The latter is the interesting part and is determined by (4.2)-(4.10). Nonetheless, the normal modes are important in interpreting the results. Such a mode is complex and has time dependence e^{st} . Modes are governed by (4.2)-(4.10) with $\tilde{\mathbf{a}}=0$ and $i\varpi$ replaced by s , leading to an

eigenvalue problem with eigenvalue s . They represent the linear dynamics of the system in the absence of vibrational forcing. Viscous damping leads to decay, i.e. $\Re(s) < 0$, but a mode also oscillates with frequency $|\Im(s)|$. A mode with small $\Re(s)$ (lightly damped) resonates when forced by vibration at frequencies ϖ close to $|\Im(s)|$. Such resonant behaviour is responsible for much of what we observe in the drop's response to different ϖ . Modes are either symmetric or antisymmetric, the former being forced by normal wall vibration, the latter by tangential vibration.

The case of small Oh is the only one for which a numerical scheme has been developed. The limit $\text{Oh} \rightarrow 0$ is analysed in section 5 and the resulting numerical implementation is described in appendices C and D (supplementary material). The analysis of section 5 brings out two distinct viscous mechanisms. One, arising from the regions near the contact lines, is characterized by a parameter β . The other comes from the boundary layer at the wall and is of order $\text{Oh}^{1/2}$. In section 7, an analysis of lightly damped modes close to resonance is given. This quantifies the effects of the two damping mechanisms, in particular allowing detailed quantification of their relative importance, which is found to depend on the contact angle and $\beta/\text{Oh}^{1/2}$.

The antisymmetric problem is rather different from the symmetric one. This is because, in the inviscid case, the drop has no means of sensing tangential wall motion. Thus, it remains in equilibrium, unaffected by vibration. Small viscosity allows vibration to affect the drop. However, in the symmetric case, the vibrations are normal to the wall and the drop is affected, even in the absence of viscosity.

Concerning the numerical results, given in section 8, figures 6-8 illustrate the importance of resonances for a particular choice of parameters. As expected, lightly damped modes resonate close to their inviscid natural frequencies, frequencies which are given in figure 5 as a function of the contact angle and in table 1 for the case $\bar{\theta} = \pi$, near which the numerical method has problems. Figures 9 and 10 quantify the coefficients associated with contact-line and boundary-layer damping as functions of the contact angle. Comparing the two damping mechanisms, the results shown in figure 11 allow quantification of their relative importance. Cases can be found in which they are comparable, and others in which one or other dominates.

Finally, comparison of the results of the theory and DNS in figures 2-4 indicates agreement for a particular case with small wall displacement amplitude. Although, owing to the high computational cost of DNS, it was only carried out for a single set of parameter values, this comparison suggests validity of both the theory, within its range of validity, and the DNS for the given contact-line model.

It would, of course, be more realistic to consider a spherical drop on a vibrating wall. The theoretical formulation of that problem, using an approach which closely follows that given here for the 2D drop, is fairly straightforward (see appendix E (supplementary material)).

However, the numerics appear to be considerably more difficult and, despite attempts in that direction, we have not yet been able to develop a numerical implementation. We continue nonetheless and expect the results for the spherical drop to be qualitatively similar to those obtained here.

Acknowledgement

This work was carried out with support from the French ANR research agency, project number ANR-15-CE08-0031, also known as ICEWET.

References

Afkhami, S., Bussmann, M., Zaleski, S., 2009. A mesh-dependent model for applying dynamic contact angles to VOF simulations. *J. Comput. Phys.* **228(15)**, 5370-5389.

Batchelor, G. K., 1967. An introduction to Fluid Dynamics. Cambridge University Press.

Bonn, D., Eggers, J., Indekeu, J., Meunier, J. and Rolley, E., 2009. Wetting and spreading. *Rev. Mod. Phys.* **81**, 739-805.

Brunet, P., Costalonga, M., 2020. Directional motion of vibrated sessile drops : A quantitative study. *Phys. Rev. Fluid* **5**, 023601.

Cox, R. G., 1986. The dynamics of the spreading of liquids on a solid surface. Part 1. Viscous flow. *J. Fluid Mech.* **168**, 169-194.

Hocking, L. M., 1977. A moving fluid interface. Part 2. The removal of the force singularity by a slip flow. *J. Fluid Mech.* **79**, 209-229.

Hocking, L. M., 1981. Sliding and spreading of thin drops. *Q. J. Mech. Appl. Math.* **34**, 37-55.

Hocking, L. M., Rivers, A. D., 1982. The spreading of a drop by capillary action. *J. Fluid Mech.* **121**, 425-442.

Hocking, L. M., 1987. The damping of capillary-gravity waves at a rigid boundary. *J. Fluid Mech.* **179**, 253-266.

Huh, C., Scriven, L. E., 1971. Hydrodynamic model of steady movement of a solid/liquid/fluid contact line. *J. Colloid. Interf. Sci.* **35**, 85-101.

Jiang, G.-S., Shu, C.-W. 1996. Efficient implementation of weighted ENO schemes. *J. Comput. Phys.* **126(1)**, 202-228.

Lamb, H., 1932. Hydrodynamics. Cambridge University Press.

Lyubimov, D. V., Lyubimova, T. P., Shklyaev, S. V. 2006 Behavior of a drop on an oscillating solid plate. *Phys. Fluids* **18(1)**, 012101.

Moffatt, H.K. 1964 Viscous and resistive eddies near a sharp corner. *J. Fluid Mech.* **18**, 1-18.

Moradi, M., Rahimian, M. H., Chini, S. F. 2019. Numerical investigation of vibration-induced droplet shedding on smooth surfaces with large contact angles. *Phys. Rev. E* **100**, 023105.

Noblin, X., Buguin, A., Brochard-Wyart, F. 2004 Vibrated sessile drops: transition between pinned and mobile contact line oscillations. *Eur. Phys. J. E* **14**(4), 395-404.

Oh, J. M., Legendre, D., Mugele, F. 2012 Shaken not stirred — On internal flow patterns in oscillating sessile drops. *Europhys. Lett.* **98**(3), 34003.

O’Naraigh, L., Valluri, P., Scott, D. M., Bethune, I., Spelt, P. D. 2014 Linear instability, nonlinear instability and ligament dynamics in three-dimensional laminar two-layer liquid flows. *J. Fluid Mech.* **750**, 464-506.

Osher, S., Shu, C.-W. 1988. Efficient implementation of essentially non-oscillatory shock-capturing schemes. *J. Comput. Phys* **77**(2), 439-471.

Lord Rayleigh 1879 On the capillary phenomena of jets. *Proc. Roy. Soc. Lond.* **29**, 71–97.

Scott, J. F. 2020 Calculation of a key function in the asymptotic description of moving contact lines. *Q. J. Mech. Appl. Math.*, **73**(4), 279-291.

Solomenko, Z., Spelt, P. D., Naraigh, L. O., Alix, P. 2017a Mass conservation and reduction of parasitic interfacial waves in level-set methods for the numerical simulation of two-phase flows: a comparative study. *Int. J. Multiph. Flow* **95**, 235-256.

Solomenko, Z., Spelt, P. D., Alix, P. 2017b A level-set method for large-scale simulations of three-dimensional flows with moving contact lines. *J. Comput. Phys.* **348**, 151-170.

Sussman, M., Smereka, P., Osher, S. 1994 A level set approach for computing solutions to incompressible two-phase flows. *J. Comput. Phys.* **148**, 81-124.

Sussman, M., Uto, S. 1998 A computational study of the spreading of oil underneath a sheet of ice. Technical Report, CAM Report 98-32, University of California, Los Angeles.

Sussman, M., Fatemi, E. 1999 An efficient, interface-preserving level set redistancing algorithm and its application to interfacial incompressible fluid flow. *SIAM J. Sci. Comput.* **20**(4), 1165-1191.

Vukasinovic, B., Smith, M. K., Glezer, A. 2007 Dynamics of a sessile drop in forced vibration. *J. Fluid Mech.* **587**, 395-423.

Appendix A: Some analytical details

A.1 Derivation of (3.4)

The definition of the interfacial unit normal vector, \mathbf{n} , can be extended away from the interface using

$$\mathbf{n} = \frac{\nabla F}{|\nabla F|}, \quad (\text{A.1})$$

which can be shown to provide the interfacial curvature via

$$\kappa = \nabla \cdot \mathbf{n} \quad (\text{A.2})$$

when the right-hand side is evaluated at the interface. Employing the definition, $F(\mathbf{x}, t) = r - \bar{r} - \eta(\chi, t)$, of F , the r and χ components of ∇F are 1 and $-r^{-1}\partial\eta/\partial\chi$, hence $|\nabla F| = \left(1 + r^{-2}(\partial\eta/\partial\chi)^2\right)^{1/2}$. Neglecting the second-order term, $|\nabla F| = 1$ correct to first order in the perturbation. It follows that the components of \mathbf{n} are

$$n_r = 1, \quad n_\chi = -\frac{1}{r} \frac{\partial\eta}{\partial\chi}, \quad (\text{A.3})$$

again correct to first order. Using the formula for the divergence in polar coordinates,

$$\nabla \cdot \mathbf{n} = \frac{1}{r} \left(\frac{\partial n_r}{\partial r} + \frac{\partial n_\chi}{\partial \chi} \right) = \frac{1}{r} - \frac{1}{r^2} \frac{\partial^2 \eta}{\partial \chi^2}, \quad (\text{A.4})$$

whose application at the interface gives

$$\kappa = \frac{1}{\bar{r} + \eta} - \frac{1}{(\bar{r} + \eta)^2} \frac{\partial^2 \eta}{\partial \chi^2}. \quad (\text{A.5})$$

The equilibrium value of κ being \bar{r}^{-1} ,

$$\kappa' = \frac{1}{\bar{r} + \eta} - \frac{1}{(\bar{r} + \eta)^2} \frac{\partial^2 \eta}{\partial \chi^2} - \frac{1}{\bar{r}}, \quad (\text{A.6})$$

which becomes (3.4) when it is recalled that η is small.

A.2 Derivation of (5.2)

Consider the boundary layer on the wall. Since the layer is thin, $\nabla^2 \sim \partial^2 / \partial y^2$ so the x -component of (4.2) gives the approximation

$$i\omega \tilde{u}_x = -\frac{\partial \tilde{p}}{\partial x} + \text{Oh} \frac{\partial^2 \tilde{u}_x}{\partial y^2}. \quad (\text{A.7})$$

Because \tilde{p} has no boundary layer, variations of $\partial \tilde{p} / \partial x$ across the layer are negligible. Since $\lambda \ll \text{Oh}^{1/2}$ and $\partial / \partial y = O(\text{Oh}^{-1/2})$, the left-hand side of the first equation in (2.4) is negligible and the wall boundary condition is (4.4). Treating $\partial \tilde{p} / \partial x$ as independent of y and using $\tilde{u}_x = 0$ at the wall, (A.7) implies

$$\tilde{u}_x = i\varpi^{-1} \frac{\partial \tilde{p}}{\partial x} \left(1 - e^{-\text{Oh}^{-1/2} (i\varpi)^{1/2} y} \right), \quad (\text{A.8})$$

where the complex square root, $(i\varpi)^{1/2}$, is a principal value to avoid exponential growth outside the layer. Using (A.8) in (4.3),

$$\frac{\partial \tilde{u}_y}{\partial y} = -i\varpi^{-1} \frac{\partial^2 \tilde{p}}{\partial x^2} \left(1 - e^{-\text{Oh}^{-1/2} (i\varpi)^{1/2} y} \right), \quad (\text{A.9})$$

whose solution, given $\tilde{u}_y = 0$ at $y = 0$, is

$$\tilde{u}_y = -i\varpi^{-1} \frac{\partial^2 \tilde{p}}{\partial x^2} \left(y - \frac{\text{Oh}^{1/2}}{(i\varpi)^{1/2}} \left(1 - e^{-\text{Oh}^{-1/2} (i\varpi)^{1/2} y} \right) \right). \quad (\text{A.10})$$

Just outside the layer, (A.10) and the y -component of (4.2), without the viscous term, give

$$\frac{\partial \tilde{p}}{\partial y} = \frac{\partial^2 \tilde{p}}{\partial x^2} \left(\frac{\text{Oh}^{1/2}}{(i\varpi)^{1/2}} - y \right). \quad (\text{A.11})$$

Since \tilde{p} has no boundary layer, this result can be applied at $y = 0$, giving (5.2).

A.3 Derivation of (5.3)

Consider the region $r - \bar{r} = O(\text{Oh}^{1/2})$, close to the liquid/gas interface and where a boundary layer similar to that near the wall might be expected, (4.2) and (4.7) give

$$i\varpi \tilde{u}_\chi = -\frac{1}{\bar{r}} \frac{\partial \tilde{p}}{\partial \chi} + \text{Oh} \frac{\partial^2 \tilde{u}_\chi}{\partial r^2}, \quad (\text{A.12})$$

$$\frac{\partial \tilde{u}_\chi}{\partial r} = 0 \quad r = \bar{r} \quad (\text{A.13})$$

at leading order. Because \tilde{p} has no boundary layer, variations of $\partial \tilde{p} / \partial \chi$ across the layer are negligible. Treating $\partial \tilde{p} / \partial \chi$ as independent of r , the solution of (A.12) and (A.13) is

$$\tilde{u}_\chi = i\varpi^{-1} \frac{1}{\bar{r}} \frac{\partial \tilde{p}}{\partial \chi}. \quad (\text{A.14})$$

Using (A.14) in (4.3),

$$\frac{\partial}{\partial r} (r \tilde{u}_r) = -i\varpi^{-1} \frac{1}{\bar{r}} \frac{\partial^2 \tilde{p}}{\partial \chi^2}. \quad (\text{A.15})$$

Integrating and using (4.5),

$$r\tilde{u}_r = i\varpi\bar{r}\tilde{\eta} - i\varpi^{-1} \frac{1}{\bar{r}} \frac{\partial^2 \tilde{p}}{\partial \chi^2} (r - \bar{r}). \quad (\text{A.16})$$

Just outside the layer, the r -component of (4.2) without the viscous term gives

$$\tilde{u}_r = i\varpi^{-1} \frac{\partial \tilde{p}}{\partial r}. \quad (\text{A.17})$$

Combining (A.16) and (A.17),

$$r \frac{\partial \tilde{p}}{\partial r} = \varpi^2 \bar{r} \tilde{\eta} - \frac{1}{\bar{r}} \frac{\partial^2 \tilde{p}}{\partial \chi^2} (r - \bar{r}), \quad (\text{A.18})$$

which, since \tilde{p} has no boundary layer, gives (5.3).

A.4 Derivation of (5.9)

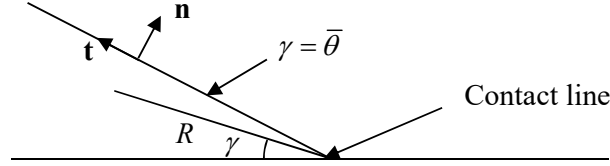


Figure A.1: Geometry and polar-coordinate system close to a contact line. The liquid/gas interface is here approximated as $\gamma = \bar{\theta}$. The drop occupies $0 \leq \gamma \leq \bar{\theta}$.

Consider the flow at distances $\text{Oh}^{1/2} \ll R \ll 1$ from one of the contact lines. Given $R \ll 1$, a first approximation of the equilibrium interface is $\gamma = \bar{\theta}$, where the polar coordinates R , γ are as indicated in figure A.1. (5.1)-(5.3) have the leading-order approximations

$$\frac{1}{R} \frac{\partial}{\partial R} \left(R \frac{\partial \tilde{p}}{\partial R} \right) + \frac{1}{R^2} \frac{\partial^2 \tilde{p}}{\partial \gamma^2} = 0, \quad (\text{A.19})$$

$$\frac{\partial \tilde{p}}{\partial \gamma} = 0 \quad \gamma = 0, \quad (\text{A.20})$$

$$\frac{1}{R} \frac{\partial \tilde{p}}{\partial \gamma} = \varpi^2 \tilde{\eta}_{\pm} \quad \gamma = \bar{\theta}. \quad (\text{A.21})$$

The solution of (A.19)-(A.21) is

$$\tilde{p} = \varpi^2 q_{\pm} R \cos \gamma \quad (\text{A.22})$$

to within an additive constant, where q_{\pm} is given by (5.10). Thus, we have the leading-order approximation

$$\frac{\partial \tilde{p}}{\partial R} = \varpi^2 q_{\pm}. \quad (\text{A.23})$$

at the wall.

(4.3) implies

$$\int_{\partial D} \tilde{\mathbf{u}} \cdot \mathbf{n} \, ds = 0, \quad (\text{A.24})$$

where D is the region $R \leq R_{\max}$ of the equilibrium drop, ∂D denotes the boundary of D , \mathbf{n} is its outward unit normal vector and s is arc length along the boundary. Since $\tilde{u}_y = 0$ at the wall, its contribution to the integral in (A.24) is zero. (4.5) gives the interfacial contribution as

$$i\varpi \int_{\partial D_i} \tilde{\eta} \, ds, \quad (\text{A.25})$$

where ∂D_i is the interfacial part of ∂D . Taking $\text{Oh}^{1/2} \ll R_{\max} \ll 1$ the contribution of the circular arc $R = R_{\max}$ can be determined as follows. Outside the wall boundary layer,

$$\tilde{\mathbf{u}} \cdot \mathbf{n} = u_R = i\varpi^{-1} \frac{\partial \tilde{p}}{\partial R}, \quad (\text{A.26})$$

where we have used (4.2) without the viscous term. Inside the boundary layer, (A.8) gives

$$\begin{aligned} \tilde{\mathbf{u}} \cdot \mathbf{n} &= i\varpi^{-1} \frac{\partial \tilde{p}}{\partial R} \left(1 - e^{-\text{Oh}^{-1/2}(i\varpi)^{1/2}y} \right) \\ &= i\varpi^{-1} \frac{\partial \tilde{p}}{\partial R} - i\varpi q_{\pm} e^{-\text{Oh}^{-1/2}(i\varpi)^{1/2}y} \end{aligned} \quad (\text{A.27})$$

at leading order, where we have used (A.23) to approximate the exponential term. Thus, the contribution of $R = R_{\max}$ to the integral in (A.24) is

$$i\varpi^{-1} \int_{\partial D_R} \frac{\partial \tilde{p}}{\partial R} \, ds - (i\varpi)^{1/2} \text{Oh}^{1/2} q_{\pm}, \quad (\text{A.28})$$

where ∂D_R is the part of ∂D with $R = R_{\max}$. Using (A.24), (A.25) with $\tilde{\eta}$ approximated by $\tilde{\eta}_{\pm}$ and (A.28),

$$\int_{\partial D_R} \frac{\partial \tilde{p}}{\partial R} \, ds = -\varpi^2 \tilde{\eta}_{\pm} R_{\max} - i\varpi (i\varpi)^{1/2} \text{Oh}^{1/2} q_{\pm}. \quad (\text{A.29})$$

Employing the coordinate system R, γ ,

$$\int_0^{\bar{\theta}} \frac{\partial \tilde{p}}{\partial R} \Big|_{R=R_{\max}} d\gamma = -\varpi^2 \tilde{\eta}_{\pm} - i\varpi (i\varpi)^{1/2} \text{Oh}^{1/2} q_{\pm} R_{\max}^{-1}. \quad (\text{A.30})$$

Since R_{\max} can take any value in the range $\text{Oh}^{1/2} \ll R_{\max} \ll 1$, (A.30) gives

$$\frac{d}{dR} \int_0^{\bar{\theta}} \tilde{p} d\gamma = -\bar{\omega}^2 \tilde{\eta}_{\pm} - i\bar{\omega} (i\bar{\omega})^{1/2} \text{Oh}^{1/2} q_{\pm} R^{-1}, \quad (\text{A.31})$$

for R in the same range. Integration of (A.31) implies (5.9).

Appendix B: Flow near the contact lines

As one of the contact lines is approached, the viscous term in (3.1) grows in importance compared with the one (representing unsteadiness) on the left-hand side. Thus, the unsteady term is neglected here. Furthermore, η can be replaced by the contact-line value $\eta_{\pm}(t)$ in (3.3), hence

$$\mathbf{u} \cdot \mathbf{n} = \frac{d\eta_{\pm}}{dt} \quad (\text{B.1})$$

on the liquid/gas interface. The interface is approximated as a flat surface of angle $\bar{\theta}$, as indicated by figure A.1, which shows the polar coordinates, R , $0 \leq \gamma \leq \bar{\theta}$, employed in this region.

Recalling that the slip region is small, we first consider the flow outside that region, where the wall boundary condition is (3.10). Thus, we suppose R small enough that unsteadiness can be neglected, but much larger than the slip length λ . The solution of (2.2), (3.1) without the unsteady term, the interfacial conditions (3.6) and (B.1) and the wall condition (3.10) is

$$u_R = -\frac{d\eta_{\pm}}{dt} \frac{1}{\bar{\theta} - \sin \bar{\theta} \cos \bar{\theta}} \frac{d}{d\gamma} (\gamma \cos(\bar{\theta} - \gamma) - \cos \bar{\theta} \sin \gamma), \quad (\text{B.2})$$

$$u_{\gamma} = \frac{d\eta_{\pm}}{dt} \frac{\gamma \cos(\bar{\theta} - \gamma) - \cos \bar{\theta} \sin \gamma}{\bar{\theta} - \sin \bar{\theta} \cos \bar{\theta}}, \quad (\text{B.3})$$

$$p' = p_{\pm} - \frac{2 \text{Oh}}{R} \frac{d\eta_{\pm}}{dt} \frac{\cos(\bar{\theta} - \gamma)}{\bar{\theta} - \sin \bar{\theta} \cos \bar{\theta}}, \quad (\text{B.4})$$

where $p_{\pm}(t)$ are unknown functions of time, one for each contact line.

Expressing $\mathbf{n} \cdot (\nabla \mathbf{u} + (\nabla \mathbf{u})^T) \cdot \mathbf{n}$ in terms of the velocity components in polar coordinates, $\mathbf{n} \cdot (\nabla \mathbf{u} + (\nabla \mathbf{u})^T) \cdot \mathbf{n} = \frac{2}{R} \left(\frac{\partial u_{\gamma}}{\partial \gamma} + u_R \right)$, which is zero according to (B.2) and (B.3). Thus, the left-hand side of (3.5) is negligible, hence, using (B.4),

$$\frac{1}{\bar{r}^2} \left(\frac{\partial^2 \eta}{\partial \chi^2} + \eta \right) = \frac{2 \text{Oh}}{R(\bar{\theta} - \sin \bar{\theta} \cos \bar{\theta})} \frac{d\eta_{\pm}}{dt} + \mathbf{a} \cdot \mathbf{x} - p_{\pm}, \quad (\text{B.5})$$

which can be rewritten as

$$\frac{1}{\bar{r}} \frac{\partial Y}{\partial \chi} = \frac{2 \text{Oh}}{R(\bar{\theta} - \sin \bar{\theta} \cos \bar{\theta})} \frac{d\eta_{\pm}}{dt} + \mathbf{a} \cdot \mathbf{x} - p_{\pm} - \frac{\eta}{\bar{r}^2}, \quad (\text{B.6})$$

where

$$Y = \frac{1}{\bar{r}} \frac{\partial \eta}{\partial \chi}. \quad (\text{B.7})$$

Since $R \ll 1$, (B.6) gives

$$\frac{\partial Y}{\partial R} = \pm \left(-\frac{2 \text{Oh}}{R(\bar{\theta} - \sin \bar{\theta} \cos \bar{\theta})} \frac{d\eta_{\pm}}{dt} + p_{\pm} + \frac{\eta_{\pm}}{\bar{r}^2} - a_x \bar{x}_{\pm} \right), \quad (\text{B.8})$$

which is integrated to obtain

$$Y = Y_0 \pm \left(-\frac{2 \text{Oh}}{\bar{\theta} - \sin \bar{\theta} \cos \bar{\theta}} \frac{d\eta_{\pm}}{dt} \ln R + \left(p_{\pm} + \frac{\eta_{\pm}}{\bar{r}^2} - a_x \bar{x}_{\pm} \right) R \right), \quad (\text{B.9})$$

where $Y_0(t)$ is as yet undetermined.

Next consider the slip region, $R = O(\lambda)$. The problem to solve differs from the one considered thus far by replacement of the wall condition (3.10) by (2.4). Rescaling spatial coordinates using λ , the problem defined by (2.2), (3.1) without the unsteady term, the interfacial conditions (3.6) and (B.1) and the wall condition (2.4) implies

$$u_R = \frac{d\eta_{\pm}}{dt} v_R(\hat{R}, \gamma; \bar{\theta}), \quad u_{\gamma} = \frac{d\eta_{\pm}}{dt} v_{\gamma}(\hat{R}, \gamma; \bar{\theta}), \quad p' = p_{\pm} + \frac{\text{Oh}}{\lambda} \frac{d\eta_{\pm}}{dt} P(\hat{R}, \gamma; \bar{\theta}), \quad (\text{B.10})$$

where $\hat{R} = R/\lambda$ and $v_R(\hat{R}, \gamma; \bar{\theta})$, $v_{\gamma}(\hat{R}, \gamma; \bar{\theta})$ and $P(\hat{R}, \gamma; \bar{\theta})$ are solely dependent on the indicated arguments (they do not depend on Oh , λ or $d\eta_{\pm}/dt$). Matching of the final equation of (B.10) and (B.4) implies

$$P(\hat{R}, \gamma; \bar{\theta}) \sim -\frac{2 \cos(\bar{\theta} - \gamma)}{\hat{R}(\bar{\theta} - \sin \bar{\theta} \cos \bar{\theta})} \quad (\text{B.11})$$

as $\hat{R} \rightarrow \infty$. This condition makes the solution for P , which is otherwise only determined up to an unknown function of time, unique.

Using $\mathbf{n} \cdot (\nabla \mathbf{u} + (\nabla \mathbf{u})^T) \cdot \mathbf{n} = \frac{2}{R} \left(\frac{\partial u_\gamma}{\partial \gamma} + u_R \right)$ and (2.2) expressed in polar coordinates, (3.5)

gives

$$\frac{\partial Y}{\partial \hat{R}} = \pm \left(\text{Oh} \frac{d\eta_\pm}{dt} \left(P(\hat{R}, \bar{\theta}; \bar{\theta}) + 2 \frac{\partial v_R}{\partial \hat{R}}(\hat{R}, \bar{\theta}; \bar{\theta}) \right) + \lambda \left(p_\pm + \frac{\eta_\pm}{\bar{r}^2} - a_x \bar{x}_\pm \right) \right) \quad (\text{B.12})$$

as the slip-region equivalent of (B.8). Integrating (B.12) and using (3.8) at $\hat{R} = 0$,

$$Y = \pm \left(\eta_\pm \frac{\cot \bar{\theta}}{\bar{r}} + \text{Oh} \frac{d\eta_\pm}{dt} I(\hat{R}; \bar{\theta}) + \lambda \left(p_\pm + \frac{\eta_\pm}{\bar{r}^2} - a_x \bar{x}_\pm \right) \hat{R} \right) \quad (\text{B.13})$$

where

$$I(\hat{R}; \bar{\theta}) = \int_0^{\hat{R}} P(\hat{R}', \bar{\theta}; \bar{\theta}) d\hat{R}' + 2 \left(v_R(\hat{R}, \bar{\theta}; \bar{\theta}) - v_R(0, \bar{\theta}; \bar{\theta}) \right). \quad (\text{B.14})$$

Matching to (B.2) implies that $v_r(\hat{R}, \bar{\theta}; \bar{\theta})$ approaches a function of $\bar{\theta}$ as $\hat{R} \rightarrow \infty$. Using this result and (B.11), (B.14) yields

$$I(\hat{R}; \bar{\theta}) \sim -\frac{2}{\bar{\theta} - \sin \bar{\theta} \cos \bar{\theta}} \left(h(\bar{\theta}) + \ln \hat{R} \right) \quad (\text{B.15})$$

as $\hat{R} \rightarrow \infty$, where determination of $h(\bar{\theta})$ requires detailed solution of the problem in the slip region. Matching of (B.13) and (B.9) determines Y_0 , hence, recalling the definition, (B.7), of Y ,

$$\frac{1}{\bar{r}} \frac{\partial \eta}{\partial \chi} = \pm \left(\eta_\pm \frac{\cot \bar{\theta}}{\bar{r}} - \frac{d\eta_\pm}{dt} \frac{2 \text{Oh}}{\bar{\theta} - \sin \bar{\theta} \cos \bar{\theta}} \ln \left(\frac{R}{\tilde{\lambda}} \right) + \left(p_\pm + \frac{\eta_\pm}{\bar{r}^2} - a_x \bar{x}_\pm \right) R \right) \quad (\text{B.16})$$

outside the slip region, where $\tilde{\lambda}(\bar{\theta}) = \lambda e^{-h(\bar{\theta})}$ is an effective slip length, which is an $O(1)$ multiple of λ , dependent on $\bar{\theta}$.

Let ε represent the order of magnitude of \mathbf{a} , as well as p' and η in the outer region. Matching of (B.4) to the outer region requires that $p_\pm = O(\varepsilon)$, while $\eta_\pm = O(\varepsilon)$ follows from the definition of η_\pm as the contact-line values of η . Thus, because $R \ll 1$, the final term in the brackets of (B.16) is negligible compared with the first one, leading to (3.9). Agreement of this result with equation (4.7) of Hocking and Rivers (1982) requires

$$h(\bar{\theta}) = Q_i(\bar{\theta}) + 1, \quad (\text{B.17})$$

where $Q_i(\bar{\theta})$ is the function defined by equation (5.10) of that article and is the subject of Scott (2020). As noted in those articles, it can only be obtained numerically. A plot of $Q_i(\bar{\theta})$ is given by Scott, while numerical values appear as tables in both articles. The values given by Scott are based on a more precise numerical scheme and should therefore be more accurate. The parameter β , defined by (5.7), can be expressed as

$$\beta = \text{Oh} \ln \left(\frac{\text{Oh}^{1/2}}{\tilde{\lambda}} \right) = \text{Oh} \left(\ln \left(\frac{\text{Oh}^{1/2}}{\lambda} \right) + Q_i(\bar{\theta}) + 1 \right). \quad (\text{B.18})$$

The following appendices were published online by IJMF as supplementary material.

Appendix C: Numerical scheme

C.1 Preliminary analysis

We first make the change of variables

$$\hat{\eta}(\chi) = \tilde{\eta}(\chi) - \eta_0 \sin \chi \quad (\text{C.1})$$

and

$$\hat{p} = \tilde{p} - \varpi^2 \eta_0 x = \tilde{p} - \varpi^2 \eta_0 r \sin \chi, \quad (\text{C.2})$$

where η_0 is such that

$$\int_{-\bar{\theta}}^{\bar{\theta}} \hat{\eta} \sin \chi d\chi = 0. \quad (\text{C.3})$$

Thus, (4.9), (5.1)-(5.4), (5.8) and (5.9) give the outer-region problem

$$\nabla^2 \hat{p} = 0, \quad (\text{C.4})$$

$$\frac{\partial \hat{p}}{\partial y} = \frac{\text{Oh}^{1/2}}{(i\varpi)^{1/2}} \frac{\partial^2 \hat{p}}{\partial x^2} \quad y = 0, \quad (\text{C.5})$$

$$\frac{\partial \hat{p}}{\partial r} = \varpi^2 \hat{\eta} \quad r = \bar{r}, \quad (\text{C.6})$$

$$\frac{1}{\bar{r}^2} \left(\frac{d^2 \hat{\eta}}{d\chi^2} + \hat{\eta} \right) = -\hat{p} + (\tilde{a}_x - \varpi^2 \eta_0) x + \tilde{a}_y y \quad r = \bar{r}, \quad (\text{C.7})$$

$$\frac{1}{\bar{r}} \frac{d\hat{\eta}}{d\chi} \rightarrow \pm \hat{\eta}_{\pm} \left(\frac{\cot \bar{\theta}}{\bar{r}} - \frac{2i\varpi\beta}{\bar{\theta} - \sin \bar{\theta} \cos \bar{\theta}} \right) - \frac{2i\varpi\beta \sin \bar{\theta}}{\bar{\theta} - \sin \bar{\theta} \cos \bar{\theta}} \eta_0, \quad (\text{C.8})$$

$$\hat{\eta} \rightarrow \hat{\eta}_{\pm} \quad (\text{C.9})$$

as $\chi \rightarrow \pm\bar{\theta}$ and

$$\int_0^{\bar{\theta}} \hat{p}(R, \gamma) d\gamma \Rightarrow -i\varpi (i\varpi)^{1/2} \text{Oh}^{1/2} q_{\pm} \ln R \quad (\text{C.10})$$

as $R \rightarrow 0$, where

$$q_{\pm} = -\frac{1}{\sin \bar{\theta}} \hat{\eta}_{\pm} \mp \eta_0 \quad (\text{C.11})$$

according to (5.10) and \Rightarrow indicates that only the logarithmic term is given. Note that (4.10) and (C.1) imply

$$\int_{-\bar{\theta}}^{\bar{\theta}} \hat{\eta} d\chi = 0. \quad (\text{C.12})$$

Note also that, when we later decompose the problem into symmetric and antisymmetric parts, $\eta_0 = 0$ for the symmetric problem because the corresponding terms in (C.1) and (C.2) are antisymmetric.

For any given $\hat{\eta}$, solution of (C.4), (C.5) without the viscous term and (C.6) yield \hat{p} correct to leading order. The resulting value of $\varpi^{-2} \hat{p}$ at the wall will be denoted ψ . The result is used in the right-hand side of (C.5) to obtain

$$\frac{\partial \hat{p}}{\partial y} = -i\varpi (i\varpi)^{1/2} \text{Oh}^{1/2} \Pi[\hat{\eta}] \quad y = 0, \quad (\text{C.13})$$

correct to $\text{Oh}^{1/2}$, where

$$\Pi[\hat{\eta}] = \frac{d^2 \psi}{dx^2}. \quad (\text{C.14})$$

(C.13) is equivalent to (5.12) and replaces (C.5) in the full problem. To simplify the notation, we henceforth drop the tilde on $\tilde{\mathbf{a}}$ and the hats on \hat{p} , $\hat{\eta}$ and $\hat{\eta}_{\pm}$.

The circular geometry of the equilibrium interface suggests the use of bipolar coordinates:

$$x = b \frac{\sinh \tau}{\cosh \tau + \cos \xi}, \quad (\text{C.15})$$

$$y = b \frac{\sin \xi}{\cosh \tau + \cos \xi}, \quad (\text{C.16})$$

where $x = \pm b = \pm \bar{r} \sin \bar{\theta}$ are the locations of the equilibrium contact lines. The coordinates τ and ξ are orthogonal. The coordinate $0 \leq \xi \leq \bar{\theta}$ takes the value $\xi = 0$ at the wall and $\xi = \bar{\theta}$

at the unperturbed interface. $-\infty < \tau < \infty$, where $\tau = \pm\infty$ represent the contact lines. The lines of constant τ are circular, as are those of constant ξ . Note that η , which is considered as a function of χ in the main text, should now be regarded as a function of τ .

(C.4) gives

$$\frac{\partial^2 p}{\partial \tau^2} + \frac{\partial^2 p}{\partial \xi^2} = 0 \quad (\text{C.17})$$

for $0 \leq \xi \leq \bar{\theta}$. At the wall, the leading-order problem, which determines ψ , has $\partial p / \partial y = 0$, while the full problem satisfies (C.13) with (C.14). Thus,

$$\frac{\partial p}{\partial \xi} = -i\varpi (i\varpi)^{1/2} \text{Oh}^{1/2} \Phi(\tau) \quad (\text{C.18})$$

for $\xi = 0$, where $\Phi = 0$ at leading order and, according to (C.14),

$$\Phi(\tau) = \frac{1}{b} \frac{d}{d\tau} \left((\cosh \tau + 1) \frac{d\psi}{d\tau} \right) \quad (\text{C.19})$$

for the full problem. (C.6) gives

$$\frac{\partial p}{\partial \xi} = \varpi^2 b f(\tau) \quad (\text{C.20})$$

for $\xi = \bar{\theta}$, where

$$f(\tau) = \frac{\eta(\tau)}{\cosh \tau + \cos \bar{\theta}}. \quad (\text{C.21})$$

(C.3) and (C.12) imply

$$\int_{-\infty}^{\infty} f(\tau) d\tau = 0, \quad (\text{C.22})$$

$$\int_{-\infty}^{\infty} \frac{\sinh \tau}{\cosh \tau + \cos \bar{\theta}} f(\tau) d\tau = 0. \quad (\text{C.23})$$

(C.7) can be split into two first-order equations as

$$\frac{d\eta}{d\tau} = f_1(\tau), \quad (\text{C.24})$$

$$\frac{dX}{d\tau} = b^2 f_2(\tau), \quad (\text{C.25})$$

where

$$f_1(\tau) = \frac{X(\tau)}{\cosh \tau + \cos \bar{\theta}}, \quad (\text{C.26})$$

$$f_2(\tau) = -\frac{P(\tau)}{\cosh \tau + \cos \bar{\theta}}, \quad (\text{C.27})$$

$$P(\tau) = p(\tau, \xi = \bar{\theta}) + \bar{r}^{-2} \eta(\tau) - \frac{b}{\cosh \tau + \cos \bar{\theta}} \left((a_x - \varpi^2 \eta_0) \sinh \tau + a_y \sin \bar{\theta} \right). \quad (\text{C.28})$$

(C.8) and (C.9) imply

$$X \rightarrow X_{\pm}, \quad (\text{C.29})$$

$$\eta \rightarrow \eta_{\pm} \quad (\text{C.30})$$

as $\tau \rightarrow \pm\infty$, where

$$X_{\pm} = \pm b \eta_{\pm} \left(\frac{\cot \bar{\theta}}{\bar{r}} - \frac{2i\varpi\beta}{\bar{\theta} - \sin \bar{\theta} \cos \bar{\theta}} \right) - \frac{2ib\varpi\beta \sin \bar{\theta}}{\bar{\theta} - \sin \bar{\theta} \cos \bar{\theta}} \eta_0. \quad (\text{C.31})$$

Define Fourier coefficients

$$p_n(\tau) = (-1)^n \frac{2}{\bar{\theta}} \int_0^{\bar{\theta}} p(\tau, \xi) \cos \frac{n\pi\xi}{\bar{\theta}} d\xi, \quad (\text{C.32})$$

where $n \geq 0$ takes on integer values. Thus, the Fourier series

$$p = \frac{1}{2} p_0 + \sum_{n=1}^{\infty} (-1)^n p_n \cos \frac{n\pi\xi}{\bar{\theta}} \quad (\text{C.33})$$

expresses p in terms of its coefficients. Multiplying equation (C.17) by $\cos \frac{n\pi\xi}{\bar{\theta}}$ and integrating over ξ , integration by parts gives

$$\int_0^{\bar{\theta}} \frac{\partial^2 p}{\partial \xi^2} \cos \frac{n\pi\xi}{\bar{\theta}} d\xi = \left[\frac{\partial p}{\partial \xi} \cos \frac{n\pi\xi}{\bar{\theta}} + p \frac{n\pi}{\bar{\theta}} \sin \frac{n\pi\xi}{\bar{\theta}} \right]_0^{\bar{\theta}} - \frac{n^2 \pi^2}{\bar{\theta}^2} \int_0^{\bar{\theta}} p \cos \frac{n\pi\xi}{\bar{\theta}} d\xi. \quad (\text{C.34})$$

Using (C.18) and (C.20),

$$\int_0^{\bar{\theta}} \frac{\partial^2 p}{\partial \xi^2} \cos \frac{n\pi\xi}{\bar{\theta}} d\xi = (-1)^n \varpi^2 b f(\tau) + i\varpi (i\varpi)^{1/2} \text{Oh}^{1/2} \Phi(\tau) - \frac{n^2 \pi^2}{\bar{\theta}^2} \int_0^{\bar{\theta}} p \cos \frac{n\pi\xi}{\bar{\theta}} d\xi. \quad (\text{C.35})$$

Thus, employing (C.17) and (C.32),

$$\frac{d^2 p_n}{d\tau^2} - \frac{n^2 \pi^2}{\bar{\theta}^2} p_n = F_n(\tau), \quad (\text{C.36})$$

where

$$F_n(\tau) = -2\varpi^2 b \bar{\theta}^{-1} f(\tau) - 2(-1)^n \bar{\theta}^{-1} i\varpi (i\varpi)^{1/2} \text{Oh}^{1/2} \Phi(\tau). \quad (\text{C.37})$$

C.2 Determination of ψ and its derivatives

Consider the leading-order problem for which only (C.17), (C.18) with $\Phi = 0$ and (C.20) are used. Given (C.22) and (C.37) with $\Phi = 0$, the solution of (C.36) which is bounded as $\tau \rightarrow \pm\infty$ is

$$p_0 = \varpi^2 \left(p_0^c - b\bar{\theta}^{-1} \int_{-\infty}^{\infty} |\tau - \tau'| f(\tau') d\tau' \right), \quad (\text{C.38})$$

$$p_n = \pi^{-1} \varpi^2 b \frac{1}{n} \int_{-\infty}^{\infty} e^{-n\pi|\tau - \tau'|/\bar{\theta}} f(\tau') d\tau' \quad n > 0, \quad (\text{C.39})$$

where p_0^c is an integration constant. Using (C.33) with $\xi = 0$,

$$\psi(\tau) = \frac{1}{2} \left(p_0^c - b\bar{\theta}^{-1} \int_{-\infty}^{\infty} |\tau - \tau'| f(\tau') d\tau' \right) - \pi^{-1} b \int_{-\infty}^{\infty} \ln \left(1 + e^{-\pi|\tau - \tau'|/\bar{\theta}} \right) f(\tau') d\tau', \quad (\text{C.40})$$

where we have summed the infinite series for $n > 0$. Differentiating (C.40),

$$\frac{1}{b} \frac{d\psi}{d\tau} = -\frac{1}{2} \bar{\theta}^{-1} \int_{-\infty}^{\infty} \tanh \left(\frac{\pi}{2\bar{\theta}} (\tau - \tau') \right) f(\tau') d\tau'. \quad (\text{C.41})$$

Integrating (C.41) by parts and using (C.22),

$$\frac{1}{b} \frac{d\psi}{d\tau} = -\frac{1}{4} \pi \bar{\theta}^{-2} \int_{-\infty}^{\infty} \frac{\sigma(\tau')}{\cosh^2 \left(\frac{\pi}{2\bar{\theta}} (\tau - \tau') \right)} d\tau', \quad (\text{C.42})$$

where

$$\sigma(\tau) = \int_{-\infty}^{\tau} f(\tau') d\tau'. \quad (\text{C.43})$$

Since $\cosh \tau = (e^\tau + e^{-\tau})/2$, (C.42) gives

$$\frac{\cosh \tau + 1}{b} \frac{d\psi}{d\tau} = -\frac{1}{8} \pi \bar{\theta}^{-2} \int_{-\infty}^{\infty} \left(\Omega_1(\tau' - \tau) e^{\tau'} + \Omega_1(\tau - \tau') e^{-\tau'} + 2\Omega_2(\tau' - \tau) \right) \sigma(\tau') d\tau' , \quad (\text{C.44})$$

where

$$\Omega_1(T) = \frac{e^{-T}}{\cosh^2\left(\frac{\pi}{2\bar{\theta}} T\right)}, \quad (\text{C.45})$$

$$\Omega_2(T) = \frac{1}{\cosh^2\left(\frac{\pi}{2\bar{\theta}} T\right)}. \quad (\text{C.46})$$

Differentiating (C.44) and using (C.19),

$$\begin{aligned} \Phi(\tau) = & -\frac{1}{8} \pi \bar{\theta}^{-2} \left(\int_{-\infty}^{\infty} \frac{\partial}{\partial \tau} (\Omega_1(\tau' - \tau)) \sigma(\tau') e^{\tau'} d\tau' + \right. \\ & \left. + \int_{-\infty}^{\infty} \frac{\partial}{\partial \tau} (\Omega_1(\tau - \tau')) \sigma(\tau') e^{-\tau'} d\tau' + 2 \int_{-\infty}^{\infty} \frac{\partial}{\partial \tau} (\Omega_2(\tau' - \tau)) \sigma(\tau') d\tau' \right). \end{aligned} \quad (\text{C.47})$$

Given

$$\frac{\partial}{\partial \tau} (\Omega(\tau' - \tau)) = -\frac{\partial}{\partial \tau'} (\Omega(\tau' - \tau)) \quad (\text{C.48})$$

for any function Ω , (C.47) gives

$$\begin{aligned} \Phi(\tau) = & \frac{1}{8} \pi \bar{\theta}^{-2} \left(\int_{-\infty}^{\infty} \frac{\partial}{\partial \tau'} (\Omega_1(\tau' - \tau)) \sigma(\tau') e^{\tau'} d\tau' + \right. \\ & \left. + \int_{-\infty}^{\infty} \frac{\partial}{\partial \tau'} (\Omega_1(\tau - \tau')) \sigma(\tau') e^{-\tau'} d\tau' + 2 \int_{-\infty}^{\infty} \frac{\partial}{\partial \tau'} (\Omega_2(\tau' - \tau)) \sigma(\tau') d\tau' \right). \end{aligned} \quad (\text{C.49})$$

(C.21), (C.43) and (C.49) provide the expression of $\Phi(\tau)$ in terms of $\eta(\tau)$ for the full problem.

C.3 The full problem

Turning attention to the full problem, the solution of (C.36) for $n = 0$ is

$$p_0 = p_0^1 \tau + p_0^2 + \frac{1}{2} \int_{-\infty}^{\infty} |\tau - \tau'| F_0(\tau') d\tau', \quad (\text{C.50})$$

where p_0^1 and p_0^2 are integration constants. The $\tau \rightarrow \pm\infty$ limits of (C.50) give

$$p_0(\tau) \sim \tau \left(p_0^1 \pm \frac{1}{2} \int_{-\infty}^{\infty} F_0(\tau') d\tau' \right) + p_0^2 \mp \frac{1}{2} \int_{-\infty}^{\infty} \tau' F_0(\tau') d\tau'. \quad (\text{C.51})$$

On the other hand, (C.10), $\ln R \sim \mp\tau$ and (C.32) imply

$$p_0(\tau) \Rightarrow \pm 2i\varpi (i\varpi)^{1/2} \text{Oh}^{1/2} \bar{\theta}^{-1} q_{\pm} \tau. \quad (\text{C.52})$$

Agreement of the terms proportional to τ in (C.51) and (C.52) gives

$$p_0^1 \pm \frac{1}{2} \int_{-\infty}^{\infty} F_0(\tau) d\tau = \pm 2i\varpi (i\varpi)^{1/2} \text{Oh}^{1/2} \bar{\theta}^{-1} q_{\pm}, \quad (\text{C.53})$$

hence

$$p_0^1 = i\varpi (i\varpi)^{1/2} \text{Oh}^{1/2} \bar{\theta}^{-1} (q_+ - q_-), \quad (\text{C.54})$$

$$\int_{-\infty}^{\infty} F_0(\tau) d\tau = 2i\varpi (i\varpi)^{1/2} \text{Oh}^{1/2} \bar{\theta}^{-1} (q_+ + q_-). \quad (\text{C.55})$$

Using (C.11), (C.22) and (C.37),

$$p_0^1 = -i\varpi \frac{(i\varpi)^{1/2} \text{Oh}^{1/2}}{\bar{\theta} \sin \bar{\theta}} (2\eta_0 \sin \bar{\theta} + \eta_+ - \eta_-), \quad (\text{C.56})$$

$$\int_{-\infty}^{\infty} \Phi(\tau) d\tau = \frac{1}{\sin \bar{\theta}} (\eta_+ + \eta_-). \quad (\text{C.57})$$

Recalling the definition of ψ as the leading-order value of $\varpi^{-2} p$ at the wall,

$$\frac{\partial \psi}{\partial R} = \varpi^{-2} \frac{\partial \hat{p}}{\partial R} = \varpi^{-2} \frac{\partial \tilde{p}}{\partial R} \pm \eta_0 \quad (\text{C.58})$$

at $y=0$, where (C.2) has been used. Taking the limit $R \rightarrow 0$ in which a contact line is approached and using (5.10), (A.23) and $\tilde{\eta}_{\pm} = \eta_{\pm} \pm \eta_0 \sin \bar{\theta}$ (which follows from (C.1)),

$$\lim_{R \rightarrow 0} \frac{\partial \psi}{\partial R} = -\frac{\eta_{\pm}}{\sin \bar{\theta}}, \quad (\text{C.59})$$

hence

$$\lim_{\tau \rightarrow \pm\infty} \left(\frac{\cosh \tau + 1}{b} \frac{\partial \psi}{\partial \tau} \right) = \pm \frac{\eta_{\pm}}{\sin \bar{\theta}}. \quad (\text{C.60})$$

Integrating (C.19) over τ and using (C.60), it follows that (C.57) is automatically satisfied. However, (C.56) provides an additional condition.

When $n \neq 0$, the solution of (C.36) which does not grow exponentially as $\tau \rightarrow \pm\infty$ is

$$p_n(\tau) = -\frac{\bar{\theta}}{2n\pi} \int_{-\infty}^{\infty} e^{-n\pi|\tau-\tau'|/\bar{\theta}} F_n(\tau') d\tau' \quad n > 0. \quad (\text{C.61})$$

Applying (C.33) with $\xi = \bar{\theta}$ and using (C.28), (C.37), (C.50) and (C.61),

$$\begin{aligned} P(\tau) = & \bar{r}^{-2} \eta(\tau) - \frac{b}{\cosh \tau + \cos \bar{\theta}} \left((a_x - \varpi^2 \eta_0) \sinh \tau + a_y \sin \bar{\theta} \right) + \\ & \frac{1}{2} \left(p_0^1 \tau + p_0^2 - \bar{\theta}^{-1} \int_{-\infty}^{\infty} |\tau - \tau'| \left(\varpi^2 b f(\tau') + i\varpi (i\varpi)^{1/2} \text{Oh}^{1/2} \Phi(\tau') \right) d\tau' \right) - , \quad (\text{C.62}) \\ & \varpi^2 b \int_{-\infty}^{\infty} G_1(\tau - \tau') f(\tau') d\tau' - i\varpi (i\varpi)^{1/2} \text{Oh}^{1/2} \int_{-\infty}^{\infty} G_2(\tau - \tau') \Phi(\tau') d\tau' \end{aligned}$$

where

$$G_1(T) = -\frac{1}{\pi} \sum_{n=1}^{\infty} n^{-1} e^{-n\pi|T|/\bar{\theta}} = \frac{1}{\pi} \ln \left(1 - e^{-\pi|T|/\bar{\theta}} \right), \quad (\text{C.63})$$

$$G_2(T) = -\frac{1}{\pi} \sum_{n=1}^{\infty} (-1)^n n^{-1} e^{-n\pi|T|/\bar{\theta}} = \frac{1}{\pi} \ln \left(1 + e^{-\pi|T|/\bar{\theta}} \right). \quad (\text{C.64})$$

Note that $G_1(T)$ and $G_2(T)$ are even functions which decay exponentially as $T \rightarrow \pm\infty$ and that $G_1(T)$ has a logarithmic singularity at $T = 0$.

Integrating (C.24) and (C.25),

$$\eta(\tau) = \eta_- + \int_{-\infty}^{\tau} f_1(\tau') d\tau', \quad (\text{C.65})$$

$$X(\tau) = X_- + b^2 \int_{-\infty}^{\tau} f_2(\tau') d\tau'. \quad (\text{C.66})$$

C.4 Symmetric/antisymmetric decomposition and numerical discretisation

As noted in the main text, the problem can be decoupled into symmetric ($a_x = 0$) and antisymmetric ($a_y = 0$) parts. In the symmetric case, η , p and Φ are even functions of τ , while $X(\tau)$ and $\sigma(\tau)$ are odd functions. In the antisymmetric case, the converse is true.

Numerical solution of the problem involves discretisation. The unknown functions $\eta(\tau)$, $P(\tau)$, $X(\tau)$, $\sigma(\tau)$ and $\Phi(\tau)$ are represented by their values

$$\eta^m = \eta(\tau_m), P^m = P(\tau_m), \Phi^m = \Phi(\tau_m) \quad -M \leq m \leq 0, \quad (\text{C.67})$$

$$X^m = X(\tau_{m+1/2}), \sigma^m = \sigma(\tau_{m+1/2}) \quad -M \leq m < 0, \quad (\text{C.68})$$

where $\tau_m = m\Delta$ and $\tau_{m+1/2} = (m+1/2)\Delta$. We have in mind that Δ is small and $\tau_M = M\Delta$ is large. There are $5M + 8$ unknowns, namely $\eta^m, X^m, P^m, \sigma^m, \Phi^m, \eta_-, X_-, \eta_0, p_0^1$ and p_0^2 . Equations (C.49), (C.62) and (C.65) are applied at $\tau = \tau_m, -M \leq m \leq 0$, whereas (C.43) and (C.66) are used at $\tau = \tau_{m+1/2}, -M \leq m < 0$. An additional equation follows from (C.31) with the lower choice of signs. In the symmetric case, $\eta_0 = 0$ and (C.22) are used, while $p_0^1 = 0$ according to (C.56) and application of (C.66) at $\tau = 0$ gives

$$2X_- + b^2 \int_{-\infty}^{\infty} f_2(\tau') d\tau' = 0, \quad (\text{C.69})$$

where $X(0) = 0$ and the fact that $f_2(\tau')$ is an even function have been used. In the antisymmetric case, $\eta^0 = \eta(0) = 0$ and (C.23) are used, while $\eta(0) = P(0) = 0$ and (C.62) at $\tau = 0$ give $p_0^2 = 0$ and (C.56) yields

$$p_0^1 = -i\varpi \frac{2(i\varpi)^{1/2} \text{Oh}^{1/2}}{\bar{\theta} \sin \bar{\theta}} (\eta_0 \sin \bar{\theta} - \eta_-). \quad (\text{C.70})$$

Thus, in either case, there are the same number of equations as unknowns.

The integrals in (C.22), (C.23), (C.43), (C.49), (C.62), (C.65), (C.66) and (C.69) are approximated as follows. They are split into contributions from inside and outside the range $|\tau| \leq \tau_M$ for (C.49), (C.62) and (C.65), whereas $|\tau| \leq \tau_{M+1/2}$ is used for (C.22), (C.23), (C.43), (C.66) and (C.69). The contribution from outside the range is approximated using large- $|\tau|$ asymptotics.

C.5 Large- $|\tau|$ contributions to the integrals

According to (C.26) and (C.29),

$$f_1(\tau) \sim 2X_{\pm} e^{-|\tau|} \quad (\text{C.71})$$

as $\tau \rightarrow \pm\infty$, hence

$$\int_{-\infty}^{-\tau_M} f_1(\tau') d\tau' \sim 2X_- e^{-\tau_M}. \quad (\text{C.72})$$

for (C.65). Using (C.30) and (C.71), integration of (C.24) leads to large- $|\tau|$ expansions for $\eta(\tau)$. The results are employed in (C.21) to obtain

$$f(\tau) \sim 2\eta_{\pm} e^{-|\tau|} - 4(\eta_{\pm} \cos \bar{\theta} \pm X_{\pm}) e^{-2|\tau|}, \quad (\text{C.73})$$

thus

$$\int_{-\infty}^{-\tau_{M+1/2}} f(\tau') d\tau' \sim 2\eta_- e^{-\tau_{M+1/2}} - 2(\eta_- \cos \bar{\theta} - X_-) e^{-2\tau_{M+1/2}} \quad (\text{C.74})$$

for (C.43). In the symmetric case, using just the first term in the expansion (C.73),

$$\int_{-\infty}^{-\tau_{M+1/2}} f(\tau) d\tau + \int_{\tau_{M+1/2}}^{\infty} f(\tau) d\tau \sim 4\eta_- e^{-\tau_{M+1/2}} \quad (\text{C.75})$$

for (C.22), while, in the antisymmetric problem,

$$\int_{-\infty}^{-\tau_{M+1/2}} \frac{\sinh \tau}{\cosh \tau + \cos \bar{\theta}} f(\tau) d\tau + \int_{\tau_{M+1/2}}^{\infty} \frac{\sinh \tau}{\cosh \tau + \cos \bar{\theta}} f(\tau) d\tau \sim -4\eta_- e^{-\tau_{M+1/2}} \quad (\text{C.76})$$

for (C.23).

As $\tau \rightarrow \pm\infty$, $p_n(\tau) \rightarrow 0$ for $n \neq 0$, while p_0 is described by (C.51). Thus, using (C.11), (C.28), (C.30), (C.33), (C.51) and (C.53),

$$P(\tau) \sim p_{\pm} + \bar{r}^{-2} \eta_{\pm} \mp b(a_x - \varpi^2 \eta_0) - i\varpi \frac{(i\varpi)^{1/2} \text{Oh}^{1/2}}{\bar{\theta} \sin \bar{\theta}} (\eta_0 \sin \bar{\theta} \pm \eta_{\pm}) \tau, \quad (\text{C.77})$$

where

$$p_{\pm} = \frac{1}{2} \left(p_0^2 \mp \frac{1}{2} \int_{-\infty}^{\infty} \tau F_0(\tau) d\tau \right). \quad (\text{C.78})$$

Using (C.77) in (C.27),

$$f_2(\tau) \sim 2e^{-|\tau|} \left(-p_{\pm} - \bar{r}^{-2} \eta_{\pm} \pm b(a_x - \varpi^2 \eta_0) + i\varpi \frac{(i\varpi)^{1/2} \text{Oh}^{1/2}}{\bar{\theta} \sin \bar{\theta}} (\eta_0 \sin \bar{\theta} \pm \eta_{\pm}) \tau \right), \quad (\text{C.79})$$

hence

$$\int_{-\infty}^{-\tau_{M+1/2}} f_2(\tau') d\tau' \sim -2\zeta e^{-\tau_{M+1/2}} \quad (\text{C.80})$$

for (C.66), where

$$\zeta = p_- + \bar{r}^{-2}\eta_- + b(a_x - \varpi^2\eta_0) + i\varpi \frac{(i\varpi)^{1/2} \text{Oh}^{1/2}}{\bar{\theta} \sin \bar{\theta}} (\tau_{M+1/2} + 1)(\eta_0 \sin \bar{\theta} - \eta_-). \quad (\text{C.81})$$

Using (C.37), (C.78) and (C.81),

$$\begin{aligned} p_0^2 &= 2\left(\zeta - \bar{r}^{-2}\eta_- - b(a_x - \varpi^2\eta_0)\right) + \\ &\bar{\theta}^{-1} \int_{-\infty}^{\infty} \tau \left(\varpi^2 b f(\tau) + i\varpi (i\varpi)^{1/2} \text{Oh}^{1/2} \Phi(\tau)\right) d\tau - . \\ &i\varpi \frac{2(i\varpi)^{1/2} \text{Oh}^{1/2}}{\bar{\theta} \sin \bar{\theta}} (\tau_{M+1/2} + 1)(\eta_0 \sin \bar{\theta} - \eta_-) \end{aligned} \quad (\text{C.82})$$

In the symmetric case, (C.80) and the fact that $f_2(\tau')$ is an even function give

$$\int_{-\infty}^{-\tau_{M+1/2}} f_2(\tau') d\tau' + \int_{\tau_{M+1/2}}^{\infty} f_2(\tau') d\tau' \sim -4\zeta e^{-\tau_{M+1/2}} \quad (\text{C.83})$$

for (C.69). Again for the symmetric problem, $a_x = \eta_0 = p_0^1 = 0$ and the integral in (C.82) is zero, hence (C.62) and (C.82) give

$$\begin{aligned} P^m &= \zeta + \bar{r}^{-2}(\eta^m - \eta_-) - \frac{b a_y \sin \bar{\theta}}{\cosh \tau_m + \cos \bar{\theta}} + i\varpi \frac{(i\varpi)^{1/2} \text{Oh}^{1/2}}{\bar{\theta} \sin \bar{\theta}} (\tau_{M+1/2} + 1)\eta_- - \\ &\frac{1}{2} \bar{\theta}^{-1} \int_{-\infty}^{\infty} |\tau_m - \tau'| \left(\varpi^2 b f(\tau') + i\varpi (i\varpi)^{1/2} \text{Oh}^{1/2} \Phi(\tau')\right) d\tau' - . \\ &\varpi^2 b \int_{-\infty}^{\infty} G_1(\tau_m - \tau') f(\tau') d\tau' - i\varpi (i\varpi)^{1/2} \text{Oh}^{1/2} \int_{-\infty}^{\infty} G_2(\tau_m - \tau') \Phi(\tau') d\tau' \end{aligned} \quad (\text{C.84})$$

In the antisymmetric case, $a_y = p_0^2 = 0$ and p_0^1 is given by (C.70), hence (C.62) yields

$$\begin{aligned} P^m &= \bar{r}^{-2}\eta^m - \frac{b(a_x - \varpi^2\eta_0) \sinh \tau_m}{\cosh \tau_m + \cos \bar{\theta}} - i\varpi \frac{(i\varpi)^{1/2} \text{Oh}^{1/2}}{\bar{\theta} \sin \bar{\theta}} \tau_m (\eta_0 \sin \bar{\theta} - \eta_-) - \\ &\frac{1}{2} \bar{\theta}^{-1} \int_{-\infty}^{\infty} |\tau_m - \tau'| \left(\varpi^2 b f(\tau') + i\varpi (i\varpi)^{1/2} \text{Oh}^{1/2} \Phi(\tau')\right) d\tau' - \\ &\varpi^2 b \int_{-\infty}^{\infty} G_1(\tau_m - \tau') f(\tau') d\tau' - i\varpi (i\varpi)^{1/2} \text{Oh}^{1/2} \int_{-\infty}^{\infty} G_2(\tau_m - \tau') \Phi(\tau') d\tau' \end{aligned} \quad (\text{C.85})$$

and (C.82) implies

$$\begin{aligned} \zeta &= \bar{r}^{-2}\eta_- + b(a_x - \varpi^2\eta_0) + i\varpi \frac{(i\varpi)^{1/2} \text{Oh}^{1/2}}{\bar{\theta} \sin \bar{\theta}} (\tau_{M+1/2} + 1)(\eta_0 \sin \bar{\theta} - \eta_-) - \\ &\frac{1}{2} \bar{\theta}^{-1} \int_{-\infty}^{\infty} \tau \left(\varpi^2 b f(\tau) + i\varpi (i\varpi)^{1/2} \text{Oh}^{1/2} \Phi(\tau)\right) d\tau \end{aligned} \quad (\text{C.86})$$

The $|\tau'| > \tau_M$ contributions to the integrals in (C.84) and (C.85) which involve $f(\tau')$ are approximated using only the first term in the expansion (C.73). Thus,

$$\int_{-\infty}^{-\tau_M} |\tau_m - \tau'| f(\tau') d\tau' + \int_{\tau_M}^{\infty} |\tau_m - \tau'| f(\tau') d\tau' \sim 4\eta_- (\tau_M + 1) e^{-\tau_M}, \quad (\text{C.87})$$

$$\begin{aligned} \int_{-\infty}^{-\tau_M} G_1(\tau_m - \tau') f(\tau') d\tau' + \int_{\tau_M}^{\infty} G_1(\tau_m - \tau') f(\tau') d\tau' \sim \\ 2\eta_- \left(e^{\tau_m} H_1(\tau_M + \tau_m) + e^{-\tau_m} H_1(\tau_M - \tau_m) \right) \end{aligned} \quad (\text{C.88})$$

in the symmetric case, while

$$\int_{-\infty}^{-\tau_M} |\tau_m - \tau'| f(\tau') d\tau' + \int_{\tau_M}^{\infty} |\tau_m - \tau'| f(\tau') d\tau' \sim 4\eta_- \tau_m e^{-\tau_M}, \quad (\text{C.89})$$

$$\begin{aligned} \int_{-\infty}^{-\tau_M} G_1(\tau_m - \tau') f(\tau') d\tau' + \int_{\tau_M}^{\infty} G_1(\tau_m - \tau') f(\tau') d\tau' \sim \\ 2\eta_- \left(e^{\tau_m} H_1(\tau_M + \tau_m) - e^{-\tau_m} H_1(\tau_M - \tau_m) \right) \end{aligned} \quad (\text{C.90})$$

for the antisymmetric problem, where

$$H_1(T) = \int_T^{\infty} G_1(T') e^{-T'} dT'. \quad (\text{C.91})$$

Likewise,

$$\int_{-\infty}^{-\tau_{M+1/2}} \tau f(\tau) d\tau + \int_{\tau_{M+1/2}}^{\infty} \tau f(\tau) d\tau \sim -4\eta_- (\tau_{M+1/2} + 1) e^{-\tau_{M+1/2}} \quad (\text{C.92})$$

for (C.86).

In the leading-order problem, $p(\tau, \xi)$ is determined by (C.17), $\partial p / \partial \xi = 0$ for $\xi = 0$ and (C.20) for $\xi = \bar{\theta}$. Using (C.73), the $\tau \rightarrow \pm\infty$ asymptotics of the leading-order $p(\tau, \xi)$ can be obtained, those of $\psi(\tau)$ deduced and (C.19) employed to find

$$\Phi(\tau) \sim \Phi_{\pm}^1 \exp(-|\tau|) + \Phi_{\pm}^2 \exp\left(-\frac{\pi - \bar{\theta}}{\bar{\theta}} |\tau|\right), \quad (\text{C.93})$$

where

$$\Phi_{\pm}^1 = -\frac{\eta_{\pm}}{\sin \bar{\theta}} \pm \frac{2X_{\pm}}{\sin 2\bar{\theta}}. \quad (\text{C.94})$$

(C.93) shows that $\Phi(\tau)$ is asymptotically the sum of two decaying exponentials, the second of which corresponds to a solution of the homogeneous problem consisting of (C.17),

$\partial p / \partial \xi = 0$ for $\xi = 0$ and $\partial p / \partial \xi = 0$ for $\xi = \bar{\theta}$. The first exponential dominates as $\tau \rightarrow \pm\infty$ for $\bar{\theta} < \pi/2$, while the second is dominant when $\bar{\theta} > \pi/2$. Uniform asymptotics needs both. Requiring that (C.93) yield $\Phi^{\pm M}$ at $\tau = \pm\tau_M$,

$$\Phi_{\pm}^2 = \exp\left(\frac{\pi - \bar{\theta}}{\bar{\theta}} \tau_M\right) \left(\Phi^{\pm M} - \Phi_{\pm}^1 e^{-\tau_M} \right). \quad (\text{C.95})$$

The case $\bar{\theta} = \pi/2$ leads to division by zero in (C.94) and must be excluded. However, this does not necessarily mean that there is a nonuniformity in the expansion (C.93) when $\bar{\theta}$ is close to $\pi/2$. If, as might be expected, $\Phi^{\pm M}$ approaches a finite limit as $\bar{\theta} \rightarrow \pi/2$, the factors multiplying the exponentials in (C.93) both tend to infinity, but in such a way that cancellation occurs.

Using (C.93),

$$\begin{aligned} & \int_{-\infty}^{-\tau_M} |\tau_m - \tau'| \Phi(\tau') d\tau' + \int_{\tau_M}^{\infty} |\tau_m - \tau'| \Phi(\tau') d\tau' \sim \\ & 2\Phi_{-}^1(\tau_M + 1) e^{-\tau_M} + \frac{2\bar{\theta}}{\pi - \bar{\theta}} \Phi_{-}^2 \left(\tau_M + \frac{\bar{\theta}}{\pi - \bar{\theta}} \right) \exp\left(-\frac{\pi - \bar{\theta}}{\bar{\theta}} \tau_M\right), \end{aligned} \quad (\text{C.96})$$

$$\begin{aligned} & \int_{-\infty}^{-\tau_M} G_2(\tau_m - \tau') \Phi(\tau') d\tau' + \int_{\tau_M}^{\infty} G_2(\tau_m - \tau') \Phi(\tau') d\tau' \sim \\ & \Phi_{-}^1 \left(e^{\tau_m} H_2(\tau_m + \tau_m) + e^{-\tau_m} H_2(\tau_m - \tau_m) \right) + \\ & \Phi_{-}^2 \left(H_3(\tau_m + \tau_m) \exp\left(\frac{\pi - \bar{\theta}}{\bar{\theta}} \tau_m\right) + H_3(\tau_m - \tau_m) \exp\left(-\frac{\pi - \bar{\theta}}{\bar{\theta}} \tau_m\right) \right) \end{aligned}, \quad (\text{C.97})$$

in the symmetric case and

$$\begin{aligned} & \int_{-\infty}^{-\tau_M} |\tau_m - \tau'| \Phi(\tau') d\tau' + \int_{\tau_M}^{\infty} |\tau_m - \tau'| \Phi(\tau') d\tau' \sim \\ & 2\Phi_{-}^1 \tau_m e^{-\tau_M} + \frac{2\bar{\theta}}{\pi - \bar{\theta}} \Phi_{-}^2 \tau_m \exp\left(-\frac{\pi - \bar{\theta}}{\bar{\theta}} \tau_M\right), \end{aligned} \quad (\text{C.98})$$

$$\begin{aligned} & \int_{-\infty}^{-\tau_M} G_2(\tau_m - \tau') \Phi(\tau') d\tau' + \int_{\tau_M}^{\infty} G_2(\tau_m - \tau') \Phi(\tau') d\tau' \sim \\ & \Phi_{-}^1 \left(e^{\tau_m} H_2(\tau_m + \tau_m) - e^{-\tau_m} H_2(\tau_m - \tau_m) \right) + \\ & \Phi_{-}^2 \left(H_3(\tau_m + \tau_m) \exp\left(\frac{\pi - \bar{\theta}}{\bar{\theta}} \tau_m\right) - H_3(\tau_m - \tau_m) \exp\left(-\frac{\pi - \bar{\theta}}{\bar{\theta}} \tau_m\right) \right) \end{aligned} \quad (\text{C.99})$$

for the antisymmetric problem, where

$$H_2(T) = \int_T^{\infty} G_2(T') e^{-T'} dT', \quad (\text{C.100})$$

$$H_3(T) = \int_T^\infty G_2(T') \exp\left(-\frac{\pi - \bar{\theta}}{\bar{\theta}} T'\right) dT'. \quad (\text{C.101})$$

Likewise, in the antisymmetric problem,

$$\begin{aligned} & \int_{-\infty}^{-\tau_{M+1/2}} \tau \Phi(\tau) d\tau + \int_{\tau_{M+1/2}}^{\infty} \tau \Phi(\tau) d\tau \sim \\ & -2\Phi_-^1(\tau_{M+1/2} + 1) e^{-\tau_{M+1/2}} - \frac{2\bar{\theta}}{\pi - \bar{\theta}} \Phi_-^2\left(\tau_{M+1/2} + \frac{\bar{\theta}}{\pi - \bar{\theta}}\right) \exp\left(-\frac{\pi - \bar{\theta}}{\bar{\theta}} \tau_{M+1/2}\right) \end{aligned} \quad (\text{C.102})$$

for (C.86).

Consider the contribution from $|\tau'| > \tau_M$ to the right-hand side of (C.49) with $\tau = \tau_m$. Using (C.22) and (C.73), (C.43) implies

$$\sigma(\tau) \sim \mp 2\eta_\pm e^{-|\tau|} + 2(X_\pm \pm \eta_\pm \cos \bar{\theta}) e^{-2|\tau|}. \quad (\text{C.103})$$

Applying this expansion and using integration by parts, the contribution of $|\tau'| > \tau_M$ to the right-hand side of (C.49) has the approximation

$$\begin{aligned} & \frac{1}{4} \pi \bar{\theta}^{-2} \left\{ (\eta_- + e^{-\tau_M} (X_- - \eta_- \cos \bar{\theta})) (\Omega_1(\tau_M + \tau_m) + \Omega_1(\tau_M - \tau_m)) + \right. \\ & \quad 2\eta_- e^{-\tau_M} (\Omega_2(\tau_M + \tau_m) + \Omega_2(\tau_M - \tau_m)) - \\ & \quad (X_- - \eta_- \cos \bar{\theta}) (e^{\tau_m} I_2(\tau_M + \tau_m) + e^{-\tau_m} I_2(\tau_M - \tau_m)) - \\ & \quad \left. 2\eta_- (e^{\tau_m} I_1(\tau_M + \tau_m) + e^{-\tau_m} I_1(\tau_M - \tau_m)) \right\} \end{aligned} \quad (\text{C.104})$$

in the symmetric case and

$$\begin{aligned} & \frac{1}{4} \pi \bar{\theta}^{-2} \left\{ (\eta_- + e^{-\tau_M} (X_- - \eta_- \cos \bar{\theta})) (\Omega_1(\tau_M + \tau_m) - \Omega_1(\tau_M - \tau_m)) + \right. \\ & \quad 2\eta_- e^{-\tau_M} (\Omega_2(\tau_M + \tau_m) - \Omega_2(\tau_M - \tau_m)) - \\ & \quad (X_- - \eta_- \cos \bar{\theta}) (e^{\tau_m} I_2(\tau_M + \tau_m) - e^{-\tau_m} I_2(\tau_M - \tau_m)) - \\ & \quad \left. 2\eta_- (e^{\tau_m} I_1(\tau_M + \tau_m) - e^{-\tau_m} I_1(\tau_M - \tau_m)) \right\} \end{aligned} \quad (\text{C.105})$$

for the antisymmetric problem, where

$$I_1(T) = \int_T^\infty \frac{e^{-T'}}{\cosh^2\left(\frac{\pi}{2\bar{\theta}} T'\right)} dT', \quad (\text{C.106})$$

$$I_2(T) = \int_T^\infty \frac{e^{-2T'}}{\cosh^2\left(\frac{\pi}{2\bar{\theta}}T'\right)} dT'. \quad (\text{C.107})$$

C.6 Completion of the numerical scheme

Turning attention to the contributions from within the ranges $|\tau| \leq \tau_M$ and $|\tau| \leq \tau_{M+1/2}$, we begin with the integral in (C.43). Taking $\tau = \tau_{m+1/2}$, $-M \leq m < 0$, the range $-\tau_{M+1/2} \leq \tau' \leq \tau_{m+1/2}$ is split into intervals, the interval l ($-M \leq l \leq m$) consisting of $\tau_{l-1/2} \leq \tau' \leq \tau_{l+1/2}$. The contribution to (C.43) from this interval is written

$$\int_{-\tau_{l-1/2}}^{\tau_{l+1/2}} f(\tau') e^{-\tau'} e^{\tau'} d\tau'. \quad (\text{C.108})$$

The quantity $f(\tau') e^{-\tau'}$ is approximated by its value, $f(\tau_l) e^{-\tau_l}$, at the centre of the interval, leading to

$$\int_{-\tau_{l-1/2}}^{\tau_{l+1/2}} f(\tau') e^{-\tau'} e^{\tau'} d\tau' = 2f(\tau_l) \sinh \frac{1}{2} \Delta. \quad (\text{C.109})$$

Summing over the intervals and combining the result with (C.74),

$$\sigma^m = 2\eta_- e^{-\tau_{M+1/2}} - 2(\eta_- \cos \bar{\theta} - X_-) e^{-2\tau_{M+1/2}} + 2 \sinh \frac{1}{2} \Delta \sum_{l=-M}^m f(\tau_l) \quad (\text{C.110})$$

is the numerical approximation of (C.43). Note that, because $f(\tau') e^{-\tau'}$ approaches a constant value at large negative τ' , the above approximation maintains precision at large negative τ_m .

The integrals in (C.22), (C.23), (C.65), (C.66), (C.69) and (C.86) are treated using the mid-point rule. (C.65), (C.66), (C.72) and (C.80) give

$$\eta^m = \eta_- + 2X_- e^{-\tau_M} + \Delta \sum_{l=-M}^{m-1} f_1(\tau_{l+1/2}), \quad (\text{C.111})$$

$$X^m = X_- - 2b^2 \zeta e^{-\tau_{M+1/2}} + \Delta b^2 \sum_{l=-M}^m f_2(\tau_l), \quad (\text{C.112})$$

where the sum in (C.111) should be interpreted as zero when $m = -M$. In the symmetric case, (C.22), (C.69), (C.75) and (C.83) yield

$$4\eta_- e^{-\tau_{M+1/2}} + \Delta \left(f(\tau_0) + 2 \sum_{l=-M}^{-1} f(\tau_l) \right) = 0, \quad (\text{C.113})$$

$$2X_- - 4b^2\zeta e^{-\tau_{M+1/2}} + \Delta b^2 \left(f_2(\tau_0) + 2 \sum_{l=-M}^{-1} f_2(\tau_l) \right) = 0. \quad (\text{C.114})$$

In the antisymmetric problem, (C.23) and (C.86) are approximated by

$$-4\eta_- e^{-\tau_{M+1/2}} + 2\Delta \sum_{l=-M}^{-1} \frac{\sinh \tau_l}{\cosh \tau_l + \cos \bar{\theta}} f(\tau_l) = 0, \quad (\text{C.115})$$

$$\begin{aligned} \zeta = & \bar{r}^{-2} \eta_- + b(a_x - \varpi^2 \eta_0) + \\ & \left(i\varpi \frac{(i\varpi)^{1/2} \text{Oh}^{1/2}}{\bar{\theta} \sin \bar{\theta}} (\eta_0 \sin \bar{\theta} - \eta_-) + 2\varpi^2 b \bar{\theta}^{-1} e^{-\tau_{M+1/2}} \eta_- \right) (\tau_{M+1/2} + 1) + \\ & i\varpi (i\varpi)^{1/2} \text{Oh}^{1/2} \bar{\theta}^{-1} \left(\Phi_-^1(\tau_{M+1/2} + 1) e^{-\tau_{M+1/2}} + \right. \\ & \left. \frac{\bar{\theta}}{\pi - \bar{\theta}} \Phi_-^2 \left(\tau_{M+1/2} + \frac{\bar{\theta}}{\pi - \bar{\theta}} \right) \exp \left(-\frac{\pi - \bar{\theta}}{\bar{\theta}} \tau_{M+1/2} \right) \right) - \\ & \Delta \bar{\theta}^{-1} \sum_{l=-M}^{-1} \tau_l \left(\varpi^2 b f(\tau_l) + i\varpi (i\varpi)^{1/2} \text{Oh}^{1/2} \Phi^l \right) \end{aligned}, \quad (\text{C.116})$$

where (C.76), (C.92) and (C.102) have been used.

In the symmetric case, the contribution to the right-hand side of (C.49) from $|\tau'| \leq \tau_M$ is

$$\begin{aligned} & \frac{1}{8} \pi \bar{\theta}^{-2} \left(\int_{-\tau_M}^0 \frac{\partial}{\partial \tau'} (\Omega_1(\tau' - \tau) + \Omega_1(\tau' + \tau)) \sigma(\tau') e^{\tau'} d\tau' + \right. \\ & \left. \int_{-\tau_M}^0 \frac{\partial}{\partial \tau'} (\Omega_1(\tau - \tau') + \Omega_1(-\tau - \tau')) \sigma(\tau') e^{-\tau'} d\tau' + \right. \\ & \left. 2 \int_{-\tau_M}^0 \frac{\partial}{\partial \tau'} (\Omega_2(\tau' - \tau) + \Omega_2(\tau' + \tau)) \sigma(\tau') d\tau' \right) \end{aligned}. \quad (\text{C.117})$$

The range $-\tau_M \leq \tau' \leq 0$ is split into intervals $\tau_l \leq \tau' \leq \tau_{l+1}$, where $-M \leq l \leq -1$. Let us consider the first integral in (C.117) with $\tau = \tau_m$. In each interval, the quantity $\sigma(\tau') e^{\tau'}$ is approximated by its value, $\sigma^l e^{\tau_{l+1/2}}$, at the centre of the interval. Thus, the contribution of the interval to (C.117) is

$$\begin{aligned} & \frac{1}{8} \pi \bar{\theta}^{-2} \int_{\tau_l}^{\tau_{l+1}} \frac{\partial}{\partial \tau'} (\Omega_1(\tau' - \tau_m) + \Omega_1(\tau' + \tau_m)) \sigma(\tau') e^{\tau'} d\tau' = \\ & \frac{1}{2} \sigma^l \left(e^{\tau_m} (e^{-\Delta/2} d_{l-m+1} - e^{\Delta/2} d_{l-m}) + e^{-\tau_m} (e^{-\Delta/2} d_{l+m+1} - e^{\Delta/2} d_{l+m}) \right) \end{aligned}, \quad (\text{C.118})$$

where $d_n = \frac{1}{4} \pi \bar{\theta}^{-2} \Omega_2(n\Delta)$. Similar reasoning applied to the second and third integrals in (C.117) gives

$$\begin{aligned} & \frac{1}{8} \pi \bar{\theta}^{-2} \int_{\tau_l}^{\tau_{l+1}} \frac{\partial}{\partial \tau'} (\Omega_1(\tau_m - \tau') + \Omega_1(-\tau_m - \tau')) \sigma(\tau') e^{-\tau'} d\tau' = \\ & \frac{1}{2} \sigma^l \left(e^{-\tau_m} (e^{\Delta/2} d_{l-m+1} - e^{-\Delta/2} d_{l-m}) + e^{\tau_m} (e^{\Delta/2} d_{l+m+1} - e^{-\Delta/2} d_{l+m}) \right) \end{aligned} \quad (\text{C.119})$$

and

$$\begin{aligned} & \frac{1}{4} \pi \bar{\theta}^{-2} \int_{\tau_l}^{\tau_{l+1}} \frac{\partial}{\partial \tau'} (\Omega_2(\tau' - \tau_m) + \Omega_2(\tau' + \tau_m)) \sigma(\tau') d\tau' = \\ & \sigma^l (d_{l-m+1} - d_{l-m} + d_{l+m+1} - d_{l+m}) \end{aligned} \quad (\text{C.120})$$

The sum of (C.118)-(C.120), followed by summation over the intervals, yields

$$\begin{aligned} & \left(\cosh \left(\left(m - \frac{1}{2} \right) \Delta \right) + 1 \right) \sum_{l=-M}^{-1} (d_{l-m+1} - d_{l+m}) \sigma^l + \\ & \left(\cosh \left(\left(m + \frac{1}{2} \right) \Delta \right) + 1 \right) \sum_{l=-M}^{-1} (d_{l+m+1} - d_{l-m}) \sigma^l \end{aligned} \quad (\text{C.121})$$

as the numerical approximation of (C.117). The sum of (C.104) and (C.121) gives the numerical expression of Φ^m for the symmetric problem. Similar treatment of the antisymmetric problem gives

$$\begin{aligned} & \left(\cosh \left(\left(m - \frac{1}{2} \right) \Delta \right) + 1 \right) \sum_{l=-M}^{-1} (d_{l-m+1} + d_{l+m}) \sigma^l - \\ & \left(\cosh \left(\left(m + \frac{1}{2} \right) \Delta \right) + 1 \right) \sum_{l=-M}^{-1} (d_{l+m+1} + d_{l-m}) \sigma^l \end{aligned} \quad (\text{C.122})$$

as the equivalent of (C.121). Thus, the sum of (C.105) and (C.122) yields Φ^m in the antisymmetric case.

With the exception of the ones involving G_1 , the contributions from $|\tau'| \leq \tau_M$ to the integrals in (C.84) and (C.85) are approximated using the trapezoidal rule. Thus, in the symmetric case,

$$\begin{aligned} & \int_{-\infty}^{\infty} |\tau_m - \tau'| f(\tau') d\tau' = 4\eta_- (\tau_M + 1) e^{-\tau_M} + \\ & \Delta \left(\tau_M f(\tau_{-M}) - \tau_m f(\tau_0) + \sum_{l=1-M}^{-1} (|\tau_m - \tau_l| + |\tau_m + \tau_l|) f(\tau_l) \right), \end{aligned} \quad (\text{C.123})$$

$$\begin{aligned}
& \int_{-\infty}^{\infty} |\tau_m - \tau'| \Phi(\tau') d\tau' = \\
& 2\Phi_-^1(\tau_M + 1)e^{-\tau_M} + \frac{2\bar{\theta}}{\pi - \bar{\theta}} \Phi_-^2\left(\tau_M + \frac{\bar{\theta}}{\pi - \bar{\theta}}\right) \exp\left(-\frac{\pi - \bar{\theta}}{\bar{\theta}} \tau_M\right) + \\
& \Delta\left(\tau_M \Phi^{-M} - \tau_m \Phi^0 + \sum_{l=1-M}^{-1} (|\tau_m - \tau_l| + |\tau_m + \tau_l|) \Phi^l\right)
\end{aligned} \tag{C.124}$$

and

$$\begin{aligned}
& \int_{-\infty}^{\infty} G_2(\tau_m - \tau') \Phi(\tau') d\tau' = \Phi_-^1\left(e^{\tau_m} H_2(\tau_M + \tau_m) + e^{-\tau_m} H_2(\tau_M - \tau_m)\right) + \\
& \Phi_-^2\left(H_3(\tau_M + \tau_m) \exp\left(\frac{\pi - \bar{\theta}}{\bar{\theta}} \tau_m\right) + H_3(\tau_M - \tau_m) \exp\left(-\frac{\pi - \bar{\theta}}{\bar{\theta}} \tau_m\right)\right) + \\
& \Delta\left(\frac{1}{2}(G_2(\tau_M + \tau_m) + G_2(\tau_M - \tau_m)) \Phi^{-M} + G_2(\tau_m) \Phi^0 + \right. \\
& \left. \sum_{l=1-M}^{-1} (G_2(\tau_m - \tau_l) + G_2(\tau_m + \tau_l)) \Phi^l\right)
\end{aligned} \tag{C.125}$$

where (C.87), (C.96) and (C.97) have been used. For the antisymmetric problem,

$$\begin{aligned}
& \int_{-\infty}^{\infty} |\tau_m - \tau'| f(\tau') d\tau' = 4\eta_- \tau_m e^{-\tau_M} + \\
& \Delta\left(\tau_m f(\tau_{-M}) + \sum_{l=1-M}^{-1} (|\tau_m - \tau_l| - |\tau_m + \tau_l|) f(\tau_l)\right),
\end{aligned} \tag{C.126}$$

$$\begin{aligned}
& \int_{-\infty}^{\infty} |\tau_m - \tau'| \Phi(\tau') d\tau' = 2\Phi_-^1 \tau_m e^{-\tau_M} + \frac{2\bar{\theta}}{\pi - \bar{\theta}} \Phi_-^2 \tau_m \exp\left(-\frac{\pi - \bar{\theta}}{\bar{\theta}} \tau_M\right) + \\
& \Delta\left(\tau_m \Phi^{-M} + \sum_{l=1-M}^{-1} (|\tau_m - \tau_l| - |\tau_m + \tau_l|) \Phi^l\right)
\end{aligned} \tag{C.127}$$

and

$$\begin{aligned}
& \int_{-\infty}^{\infty} G_2(\tau_m - \tau') \Phi(\tau') d\tau' = \Phi_-^1\left(e^{\tau_m} H_2(\tau_M + \tau_m) - e^{-\tau_m} H_2(\tau_M - \tau_m)\right) + \\
& \Phi_-^2\left(H_3(\tau_M + \tau_m) \exp\left(\frac{\pi - \bar{\theta}}{\bar{\theta}} \tau_m\right) - H_3(\tau_M - \tau_m) \exp\left(-\frac{\pi - \bar{\theta}}{\bar{\theta}} \tau_m\right)\right) + \\
& \Delta\left(\frac{1}{2}(G_2(\tau_M + \tau_m) - G_2(\tau_M - \tau_m)) \Phi^{-M} + \right. \\
& \left. \sum_{l=1-M}^{-1} (G_2(\tau_m - \tau_l) - G_2(\tau_m + \tau_l)) \Phi^l\right)
\end{aligned} \tag{C.128}$$

where (C.89), (C.98) and (C.99) have been employed. Recalling that the quantities Φ_-^1 and Φ_-^2 are given by (C.94) and (C.95), (C.123)-(C.128) express all integrals in (C.84) and (C.85), apart from the one containing G_1 , in terms of the unknowns of the problem.

The logarithmic singularity of $G_1(T)$ at $T=0$ means that more care is needed when approximating the corresponding integrals in (C.84) and (C.85). We temporarily suspend symmetry considerations, then specialize later to the symmetric and antisymmetric cases. The range $|\tau| \leq \tau_M$ is split into intervals indexed by $-M \leq l < M$, where the interval with index l is defined by $\tau_l \leq \tau' \leq \tau_{l+1}$. In each such interval, $f(\tau')$ is approximated by

$$f(\tau') = a_l + b_l e^{-|\tau_m - \tau'|}, \quad (\text{C.129})$$

where

$$a_l = \frac{f(\tau_{l+1})e^{-|\tau_m - \tau_l|} - f(\tau_l)e^{-|\tau_m - \tau_{l+1}|}}{e^{-|\tau_m - \tau_l|} - e^{-|\tau_m - \tau_{l+1}|}}, \quad (\text{C.130})$$

$$b_l = \frac{f(\tau_l) - f(\tau_{l+1})}{e^{-|\tau_m - \tau_l|} - e^{-|\tau_m - \tau_{l+1}|}} \quad (\text{C.131})$$

in order to match the values of $f(\tau)$ at $\tau = \tau_l$ and $\tau = \tau_{l+1}$. (C.129) leads to

$$\int_{-\tau_M}^{\tau_M} G_1(\tau_m - \tau') f(\tau') d\tau' = \sum_{l=-M}^{M-1} a_l (J(\tau_{l+1} - \tau_m) - J(\tau_l - \tau_m)) + \sum_{l=-M}^{M-1} b_l s_{l-m} (H_1(|\tau_l - \tau_m|) - H_1(|\tau_{l+1} - \tau_m|)) \quad (\text{C.132})$$

where $s_n = 1$ when $n \geq 0$, $s_n = -1$ when $n < 0$ and

$$J(T) = \int_0^T G_1(T') dT'. \quad (\text{C.133})$$

Using (C.130) and (C.131), (C.132) gives

$$\int_{-\tau_M}^{\tau_M} G_1(\tau_m - \tau') f(\tau') d\tau' = \sum_{l=-M}^{M-1} (c_{ml} f(\tau_l) + c_{-m, -l-1} f(\tau_{l+1})), \quad (\text{C.134})$$

where

$$c_{ml} = \frac{1}{e^{-|\tau_m - \tau_l|} - e^{-|\tau_m - \tau_{l+1}|}} \left(e^{-|\tau_m - \tau_{l+1}|} (J(\tau_l - \tau_m) - J(\tau_{l+1} - \tau_m)) + s_{l-m} (H_1(|\tau_l - \tau_m|) - H_1(|\tau_{l+1} - \tau_m|)) \right) \quad (\text{C.135})$$

and we have used $s_{m-l-1} = -s_{l-m}$ and the fact that $J(-T) = -J(T)$, which follows from $G_1(T) = G_1(-T)$ and (C.133). (C.134) can be rewritten as

$$\int_{-\tau_M}^{\tau_M} G_1(\tau_m - \tau') f(\tau') d\tau' = c_{m,-M} f(\tau_{-M}) + c_{-m,-M} f(\tau_M) + \sum_{l=1-M}^{M-1} (c_{ml} + c_{-m,-l}) f(\tau_l) \quad (\text{C.136})$$

In the symmetric case, (C.136) gives

$$\int_{-\infty}^{\infty} G_1(\tau_m - \tau') f(\tau') d\tau' = 2\eta_- \left(e^{\tau_m} H_1(\tau_M + \tau_m) + e^{-\tau_m} H_1(\tau_M - \tau_m) \right) + (c_{m,-M} + c_{-m,-M}) f(\tau_{-M}) + (c_{m0} + c_{-m,0}) f(\tau_0) + \sum_{l=1-M}^{-1} (c_{ml} + c_{-m,-l} + c_{m,-l} + c_{-m,l}) f(\tau_l) \quad (\text{C.137})$$

while

$$\int_{-\infty}^{\infty} G_1(\tau_m - \tau') f(\tau') d\tau' = 2\eta_- \left(e^{\tau_m} H_1(\tau_M + \tau_m) - e^{-\tau_m} H_1(\tau_M - \tau_m) \right) + (c_{m,-M} - c_{-m,-M}) f(\tau_{-M}) + \sum_{l=1-M}^{-1} (c_{ml} + c_{-m,-l} - c_{m,-l} - c_{-m,l}) f(\tau_l) \quad (\text{C.138})$$

in the antisymmetric case. Note that (C.88) and (C.90) have been used to express the large- $|\tau|$ contributions in (C.137) and (C.138).

The full numerical problem uses (C.31), with the lower choice of signs, and (C.110)-(C.112). In the symmetric case, $\eta_0 = 0$, (C.113) and (C.114) are applied and Φ^m is given by the sum of (C.104) and (C.121). (C.84) is used, the integrals being expressed by (C.123)-(C.125) and (C.137) with Φ_-^1 and Φ_-^2 given by (C.94) and (C.95). For the antisymmetric problem, $\eta^0 = 0$, (C.115) and (C.116) are used with Φ_-^1 , Φ_-^2 given by (C.94) and (C.95), while Φ^m is given by the sum of (C.105) and (C.122). (C.85) is applied with the integrals expressed using (C.126)-(C.128) and (C.138) and Φ_-^1 , Φ_-^2 given by (C.94) and (C.95). Thus, in either case, there are $5M + 7$ equations for the same number of unknowns, namely η^m , X^m , P^m , σ^m , Φ^m , η_- , X_- , ζ and η_0 . The number of equations and unknowns are reduced by elimination as follows. Φ^m can be eliminated using the numerical approximation of (C.49) ((C.104) and (C.121) in the symmetric case, (C.105) and (C.122) for the antisymmetric problem), σ^m using (C.110), η^m using (C.111) and X^m using (C.112). This leaves $M + 5$ equations in the same number of unknowns. In the symmetric problem, $\eta_0 = 0$ is used to eliminate η_0 , hence reducing the number to $M + 4$. For the antisymmetric case,

$P^0 = 0$ follows from (C.85) with $m = 0$. Thus, that equation and the unknown P^0 can be eliminated, reducing the number of unknowns to $M + 4$, as for the symmetric case. The resulting symmetric and antisymmetric problems can be expressed in the matrix form (5.13), where the vector U consists of $P^{-M}, P^{1-M}, \dots, P^0, \eta_-, X_-, \zeta$ for the symmetric problem and $P^{-M}, P^{1-M}, \dots, P^{-1}, \eta_-, X_-, \zeta, \eta_0$ for the antisymmetric one. In the antisymmetric case, the inviscid solution is $P^m = \eta_- = X_- = \zeta = 0, \eta_0 = \varpi^{-2} a_x$. This vector is denoted $U = \varpi^{-2} a_x V$ in the main text. Thus, V is a constant vector all of whose components are zero, apart from the one corresponding to η_0 , which is 1.

The determination of the functions $H_1(T), H_2(T), H_3(T), I_1(T), I_2(T)$ and $J(T)$ is described in appendix D.

Appendix D: Calculation of $H_1(T), H_2(T), H_3(T), I_1(T), I_2(T)$ and $J(T)$

$H_1(T), H_2(T), H_3(T), I_1(T)$ and $I_2(T)$ are required for $T = 0, \Delta, \dots, 2M\Delta$. First consider the calculation of $H_1(T)$. Let

$$F(T) = H_1(T) + (1 - e^{-T})G_1(T) \quad T \geq 0, \quad (\text{D.1})$$

then (C.63) and (C.91) imply

$$\frac{dF}{dT} = h_1(T), \quad (\text{D.2})$$

where

$$h_1(T) = \frac{e^{-\pi T / \bar{\theta}} (1 - e^{-T})}{\bar{\theta} (1 - e^{-\pi T / \bar{\theta}})} \quad (\text{D.3})$$

has the virtue of having no singularity as $T \rightarrow 0$. However, as we shall see, its value at $T = 0$ is required. Evaluated directly, (D.3) gives a zero-by-zero division, so this value is determined by taking the limit $T \rightarrow 0$.

Using (C.91) and the first equality in (C.63), we find

$$H_1(T) = -\frac{1}{\pi} \sum_{n=1}^{\infty} \frac{\exp\left(-\left(n\pi / \bar{\theta} + 1\right)T\right)}{n\left(n\pi / \bar{\theta} + 1\right)} \quad T \geq 0. \quad (\text{D.4})$$

Taking $T = 2M\Delta$, presumed large, the series in (D.4) is rapidly convergent and can be calculated numerically by truncation. This allows the determination of $F(2M\Delta)$ using (D.1). Employing Simpson's integration rule, the integral of (D.2) implies

$$F((m-1)\Delta) = F(m\Delta) - \frac{1}{6}\Delta \left(h_1((m-1)\Delta) + 4h_1\left(\left(m - \frac{1}{2}\right)\Delta\right) + h_1(m\Delta) \right), \quad (\text{D.5})$$

which can be used to determine the remaining $F(T)$. As noted above, $h_1(0)$ is needed, the $T \rightarrow 0$ limit of (D.3) giving

$$h_1(0) = \frac{1}{\pi}. \quad (\text{D.6})$$

The required $H_1(T)$ follow from (D.1) for $T > 0$. As $T \rightarrow 0$, (D.1) implies $H_1(0) = F(0)$.

Using the first equality of (C.64) in (C.100) and (C.101),

$$H_2(T) = -\frac{1}{\pi} \sum_{n=1}^{\infty} (-1)^n \frac{\exp\left(-\left(n\pi/\bar{\theta} + 1\right)T\right)}{n\left(n\pi/\bar{\theta} + 1\right)}, \quad (\text{D.7})$$

$$H_3(T) = -\frac{1}{\pi} \sum_{n=1}^{\infty} (-1)^n \frac{\exp\left(-\left((n+1)\pi/\bar{\theta} - 1\right)T\right)}{n\left((n+1)\pi/\bar{\theta} - 1\right)} \quad (\text{D.8})$$

for $T \geq 0$. Taking $T = 2M\Delta$, the series in (D.7) and (D.8) are rapidly convergent and can be calculated by truncation. (C.100), (C.101) and Simpson's rule imply

$$H_2((m-1)\Delta) = H_2(m\Delta) + \frac{1}{6}\Delta \left(h_2((m-1)\Delta) + 4h_2\left(\left(m - \frac{1}{2}\right)\Delta\right) + h_2(m\Delta) \right), \quad (\text{D.9})$$

$$H_3((m-1)\Delta) = H_3(m\Delta) + \frac{1}{6}\Delta \left(h_3((m-1)\Delta) + 4h_3\left(\left(m - \frac{1}{2}\right)\Delta\right) + h_3(m\Delta) \right), \quad (\text{D.10})$$

where

$$h_2(T) = e^{-T}G_2(T), \quad h_3(T) = e^{-(\pi-\bar{\theta})T/\bar{\theta}}G_2(T). \quad (\text{D.11})$$

Using (D.7) and (D.8) for $T = 2M\Delta$, the remaining $H_2(T)$ and $H_3(T)$ follow from (D.9) and (D.10).

Turning attention to (C.106) and (C.107), integration by parts gives

$$I_1(T) = \frac{2\bar{\theta}}{\pi} \left(\int_T^\infty e^{-T'} \tanh\left(\frac{\pi}{2\bar{\theta}} T'\right) dT' - e^{-T} \tanh\left(\frac{\pi}{2\bar{\theta}} T\right) \right), \quad (\text{D.12})$$

$$I_2(T) = \frac{2\bar{\theta}}{\pi} \left(2 \int_T^\infty e^{-2T'} \tanh\left(\frac{\pi}{2\bar{\theta}} T'\right) dT' - e^{-2T} \tanh\left(\frac{\pi}{2\bar{\theta}} T\right) \right). \quad (\text{D.13})$$

Using

$$\tanh\left(\frac{\pi}{2\bar{\theta}} T\right) = 1 + 2 \sum_{n=1}^{\infty} (-1)^n \exp\left(-\frac{n\pi}{\bar{\theta}} T\right), \quad (\text{D.14})$$

$$I_1(T) = \frac{2\bar{\theta}}{\pi} \left(e^{-T} \left(1 - \tanh\left(\frac{\pi}{2\bar{\theta}} T\right) \right) + 2 \sum_{n=1}^{\infty} (-1)^n \frac{\exp\left(-\left(n\pi/\bar{\theta} + 1\right)T\right)}{n\pi/\bar{\theta} + 1} \right), \quad (\text{D.15})$$

$$I_2(T) = \frac{2\bar{\theta}}{\pi} \left(e^{-2T} \left(1 - \tanh\left(\frac{\pi}{2\bar{\theta}} T\right) \right) + 4 \sum_{n=1}^{\infty} (-1)^n \frac{\exp\left(-\left(n\pi/\bar{\theta} + 2\right)T\right)}{n\pi/\bar{\theta} + 2} \right) \quad (\text{D.16})$$

are determined at $T = 2M\Delta$ by truncation. Applying Simpson's rule,

$$I_1((m-1)\Delta) = I_1(m\Delta) + \frac{1}{6}\Delta \left(h_4((m-1)\Delta) + 4h_4\left(\left(m-\frac{1}{2}\right)\Delta\right) + h_4(m\Delta) \right), \quad (\text{D.17})$$

$$I_2((m-1)\Delta) = I_2(m\Delta) + \frac{1}{6}\Delta \left(h_5((m-1)\Delta) + 4h_5\left(\left(m-\frac{1}{2}\right)\Delta\right) + h_5(m\Delta) \right), \quad (\text{D.18})$$

where

$$h_4(T) = \frac{e^{-T}}{\cosh^2\left(\frac{\pi}{2\bar{\theta}} T\right)}, \quad h_5(T) = \frac{e^{-2T}}{\cosh^2\left(\frac{\pi}{2\bar{\theta}} T\right)}. \quad (\text{D.19})$$

Using (D.15) and (D.16) for $T = 2M\Delta$, the remaining $I_1(T)$ and $I_2(T)$ follow from (D.17) and (D.18).

Finally, $J(T)$ is defined by (C.133) and has the limiting value $J(0) = 0$. The values of $J(n\Delta)$ are required for $-2M \leq n \leq 2M$. Since $G_1(-T) = G_1(T)$, $J(-T) = -J(T)$ and we restrict attention to $T > 0$. We have

$$J(T) = \frac{1}{\pi} \int_0^T \ln\left(1 - e^{-\pi T'/\bar{\theta}}\right) dT'. \quad (\text{D.20})$$

Changing integration variable to $z' = 1 - e^{-\pi T / \bar{\theta}}$,

$$J(T) = \frac{\bar{\theta}}{\pi^2} g\left(1 - e^{-\pi T / \bar{\theta}}\right), \quad (\text{D.21})$$

where

$$g(z) = \int_0^z \frac{\ln z'}{1-z'} dz'. \quad (\text{D.22})$$

Integrating by parts,

$$g(z) = -\ln z \ln(1-z) + \int_0^z \frac{\ln(1-z')}{z'} dz'. \quad (\text{D.23})$$

Changing integration variable to $w = 1 - z'$,

$$\int_0^z \frac{\ln(1-z')}{z'} dz' = \int_{1-z}^1 \frac{\ln w}{1-w} dw = g(1) - g(1-z), \quad (\text{D.24})$$

hence

$$g(z) + g(1-z) = g(1) - \ln z \ln(1-z). \quad (\text{D.25})$$

We have

$$\begin{aligned} g(z) &= \int_0^z \frac{\ln z'}{1-z'} dz' = -\int_0^z \sum_{n=1}^{\infty} n^{-1} (1-z')^{n-1} dz' \\ &= \sum_{n=1}^{\infty} n^{-2} \left((1-z)^n - 1 \right) = \sum_{n=1}^{\infty} n^{-2} (1-z)^n - \frac{\pi^2}{6}. \end{aligned} \quad (\text{D.26})$$

It follows that $g(1) = -\pi^2 / 6$ so (D.25) gives

$$g(z) + g(1-z) = -\frac{\pi^2}{6} - \ln z \ln(1-z). \quad (\text{D.27})$$

The series $\sum_{n=1}^{\infty} n^{-2} (1-z)^n$ converges quite rapidly when $1/2 \leq z \leq 1$ and can be numerically calculated by truncation, leading to $g(z)$ via (D.26). When $0 < z < 1/2$, (D.26) with series truncation is used to calculate $g(1-z)$ and $g(z)$ determined from (D.27).

Appendix E: Theoretical formulation for a spherical drop

This appendix gives a brief description of the formulation of the linearized, small-Oh, outer-region problem for a spherical drop. No numerical implementation of this analysis has so far been developed.

Define Cartesian coordinates x, y, z with the wall at $z = 0$ and the drop in $z > 0$, as well as spherical polar coordinates r, χ, ϕ with origin at the equilibrium drop centre, for which $x = r \sin \chi \cos \phi$, $y = r \sin \chi \sin \phi$, $z = r \cos \chi - \bar{r} \cos \bar{\theta}$, where \bar{r} is the equilibrium drop radius and $\bar{\theta}$ the contact angle. The liquid/gas interface of the equilibrium drop lies at $r = \bar{r}$, while the perturbed interface is $r = \bar{r} + \eta(\chi, \phi, t)$.

The linearized, small-Oh equations and boundary conditions of the outer problem with sinusoidal wall vibration are

$$\nabla^2 \tilde{p} = 0 \quad (\text{E.1})$$

inside the equilibrium drop,

$$\frac{\partial \tilde{p}}{\partial z} = \frac{\text{Oh}^{1/2}}{(i\varpi)^{1/2}} \left(\frac{\partial^2 \tilde{p}}{\partial x^2} + \frac{\partial^2 \tilde{p}}{\partial y^2} \right) \quad (\text{E.2})$$

for $z = 0$,

$$\frac{\partial \tilde{p}}{\partial r} = \varpi^2 \tilde{\eta}, \quad (\text{E.3})$$

$$\frac{1}{\bar{r}^2} \left(\frac{1}{\sin \chi} \frac{\partial}{\partial \chi} \left(\sin \chi \frac{\partial \tilde{\eta}}{\partial \chi} \right) + \frac{1}{\sin^2 \chi} \frac{\partial^2 \tilde{\eta}}{\partial \phi^2} + 2\tilde{\eta} \right) = -\tilde{p} + \tilde{\mathbf{a}} \cdot \mathbf{x}, \quad (\text{E.4})$$

on the equilibrium interface, $r = \bar{r}$,

$$\frac{1}{\bar{r}} \frac{\partial \tilde{\eta}}{\partial \chi} \rightarrow \tilde{\eta}_c \left(\frac{\cot \bar{\theta}}{\bar{r}} - \frac{2i\varpi\beta}{\bar{\theta} - \sin \bar{\theta} \cos \bar{\theta}} \right), \quad (\text{E.5})$$

$$\tilde{\eta} \rightarrow \tilde{\eta}_c \quad (\text{E.6})$$

as $\chi \rightarrow \bar{\theta}$ and

$$\int_0^{\bar{\theta}} \tilde{p}(R, \gamma, \phi) d\gamma \Rightarrow -i\varpi (i\varpi)^{1/2} \text{Oh}^{1/2} q \ln R \quad (\text{E.7})$$

as $R \rightarrow 0$, where R is distance from the contact line and

$$q = -\frac{\tilde{\eta}_c}{\sin \bar{\theta}}. \quad (\text{E.8})$$

That the equilibrium and perturbed drops have the same nondimensional volume is expressed by

$$\int_0^{\bar{\theta}} \int_0^{2\pi} \tilde{\eta} \sin \chi d\phi d\chi = 0. \quad (\text{E.9})$$

Equations (E.1)-(E.9) are respectively the spherical-drop equivalents of (5.1)-(5.4), (5.8), (4.9), (5.9), (5.10) and (4.10).

The solution of (E.1)-(E.9) can be expressed as a linear combination of three components: a) $\tilde{a}_x = \tilde{a}_y = 0$, $\tilde{a}_z = 1$, b) $\tilde{a}_x = \tilde{a}_z = 0$, $\tilde{a}_y = 1$, c) $\tilde{a}_x = \tilde{a}_z = 0$, $\tilde{a}_y = 1$. Component a is axisymmetric, i.e. \tilde{p} and $\tilde{\eta}$ are independent of ϕ . For components b and c,

$$\tilde{p} = (\hat{p}(r, \chi) + \varpi^2 \eta_0 r \sin \chi) f(\phi), \quad (\text{E.10})$$

$$\tilde{\eta} = (\hat{\eta}(\chi) + \eta_0 \sin \chi) f(\phi), \quad (\text{E.11})$$

$$\tilde{\eta}_c = (\hat{\eta}_c + \eta_0 \sin \bar{\theta}) f(\phi), \quad (\text{E.12})$$

$$q = \hat{q} f(\phi), \quad (\text{E.13})$$

where $f(\phi) = \cos \phi$ for component b, $f(\phi) = \sin \phi$ for component c, and the constant η_0 is chosen such that

$$\int_0^{\bar{\theta}} \hat{\eta} \sin \chi d\chi = 0. \quad (\text{E.14})$$

It should be noted that \hat{p} , $\hat{\eta}$, $\hat{\eta}_c$, η_0 and \hat{q} are the same for components b and c. In what follows, $p = \tilde{p}$, $\eta = \tilde{\eta}$, $\eta_c = \tilde{\eta}_c$ and $\eta_0 = 0$ for component a, while $p = \hat{p}$, $\eta = \hat{\eta}$, $\eta_c = \hat{\eta}_c$ and $q = \hat{q}$ for components b and c.

Equation (E.1) yields

$$\frac{1}{r^2} \frac{\partial}{\partial r} \left(r^2 \frac{\partial p}{\partial r} \right) + \frac{1}{r^2 \sin \chi} \frac{\partial}{\partial \chi} \left(\sin \chi \frac{\partial \tilde{\eta}}{\partial \chi} \right) - \frac{k^2}{r^2 \sin^2 \chi} p = 0 \quad (\text{E.15})$$

inside the equilibrium drop, where $k = 0$ for component a and $k = 1$ for components b and c. (E.2) gives

$$\frac{\partial p}{\partial z} = \frac{\text{Oh}^{1/2}}{(i\varpi)^{1/2}} \left(\frac{1}{\rho} \frac{\partial}{\partial \rho} \left(\rho \frac{\partial p}{\partial \rho} \right) - \frac{k^2}{\rho^2} p \right) \quad (\text{E.16})$$

on $z = 0$, where p is here regarded as a function of the cylindrical coordinates, z and $\rho = (x^2 + y^2)^{1/2} = r \sin \chi$, the distance to the drop axis. (E.3) and (E.4) imply

$$\frac{\partial p}{\partial r} = \varpi^2 \eta, \quad (\text{E.17})$$

$$\frac{1}{\bar{r}^2} \left(\frac{1}{\sin \chi} \frac{d}{d\chi} \left(\sin \chi \frac{d\eta}{d\chi} \right) + \left(2 - \frac{k^2}{\sin^2 \chi} \right) \eta \right) = -p + (1 - \varpi^2 \eta_0) \bar{r} \sigma_k(\chi) \quad (\text{E.18})$$

when $r = \bar{r}$, where $\sigma_0(\chi) = \cos \chi - \cos \bar{\theta}$ and $\sigma_1(\chi) = \sin \chi$. (E.5) and (E.6) yield

$$\frac{1}{\bar{r}} \frac{d\eta}{d\chi} \rightarrow \eta_c \left(\frac{\cot \bar{\theta}}{\bar{r}} - \frac{2i\varpi\beta}{\bar{\theta} - \sin \bar{\theta} \cos \bar{\theta}} \right) - \frac{2i\varpi\beta \sin \bar{\theta}}{\bar{\theta} - \sin \bar{\theta} \cos \bar{\theta}} \eta_0, \quad (\text{E.19})$$

$$\eta \rightarrow \eta_c \quad (\text{E.20})$$

as $\chi \rightarrow \bar{\theta}$. (E.7) and (E.8) give

$$\int_0^{\bar{\theta}} p(R, \gamma) d\gamma \Rightarrow i\varpi (i\varpi)^{1/2} \text{Oh}^{1/2} \left(\frac{\eta_c}{\sin \bar{\theta}} + \eta_0 \right) \ln R \quad (\text{E.21})$$

as $R \rightarrow 0$. (E.9) is automatically satisfied for components b and c. (E.9) when $k = 0$ and (E.14) when $k = 1$ imply

$$\int_0^{\bar{\theta}} \eta \sin \chi d\chi = 0. \quad (\text{E.22})$$

As in the 2D problem, a leading-order relation for p can be obtained using (E.15), (E.16) with $\text{Oh} = 0$ (i.e. $\partial p / \partial z = 0$ when $z = 0$) and (E.17). Furthermore, (E.21) with $\text{Oh} = 0$ implies that there is no logarithmic singularity in the leading-order problem. None of the other equations are applied in that problem. The resulting value of $\varpi^{-2} p$ at the wall is denoted $\psi(\rho)$. The result is used in (E.16) to obtain

$$\frac{\partial p}{\partial z} = -i\varpi (i\varpi)^{1/2} \text{Oh}^{1/2} \left(\frac{1}{\rho} \frac{d}{d\rho} \left(\rho \frac{d\psi}{d\rho} \right) - \frac{k^2}{\rho^2} \psi \right) \quad (\text{E.23})$$

for $z = 0$. In the full problem, (E.16) is replaced by (E.23) and (E.15), (E.17)-(E.22) apply.

For component a, (E.21) is automatically satisfied given the other equations of the problem. To show this, (E.1) is integrated over the equilibrium drop volume, excluding a small region $R < R_0$, and the divergence theorem is used to turn the volume integral into a surface integral. (E.17) and (E.22) imply that the interfacial contribution is zero in the limit $R_0 \rightarrow 0$. (E.23) provides the wall contribution when multiplied by $2\pi\rho$ and integrated over ρ from $\rho = 0$ to the contact-line location, $\rho = \bar{r} \sin \bar{\theta}$. Integration by parts brings in the limiting value of $\rho d\psi / d\rho$ at the contact line. Analysis of the leading-order problem as $R \rightarrow 0$ shows that $\rho d\psi / d\rho \rightarrow -q\bar{r} \sin \bar{\theta}$, with q given by (E.8). This allows evaluation of

the contribution from the wall. The remaining contribution comes from $R = R_0$ and involves the integral on the left-hand side of (E.21). The result is (E.21), which is thus automatically satisfied and is therefore dropped when $k = 0$. It is however needed when $k = 1$.